Ultra-Low Frequency Oscillation Damping Control Method for Hydro-Photovoltaic Integrated Systems

Sijia Wang, Yin Xu, *Senior Member, IEEE*, Xiangyu Wu, *Senior Member, IEEE*, Jiaxuan Wang, Gang Chen, and Xueyang Zeng

***Abstract*—In recent years, ultra-low frequency oscillations (ULFOs) have occurred in power systems with a high proportion of hydropower, which seriously threatens the system stability. With the rapid increase of the proportion of photovoltaic (PV) plants in the power grid, it is feasible to use the regulation ability of PV plants to suppress ULFOs. First, the inadaptability of the traditional Phillips–Heffron model in the analysis of ULFOs is pointed out. Second, a frequency response model of hydro-PV integrated systems is established, and a PV supplementary damping control method for suppressing ULFOs is proposed on the basis of this model. Third, the frequency response model is extended to multihydropower and multi-PV systems, and the supplementary damping control parameters of multiple PV plants are designed collaboratively. Finally, time-domain simulation and experimental results validate the effectiveness of the proposed method.**

***Index Terms*—Damping torque, frequency oscillation, hydropower generator, photovoltaic (PV) plant, primary frequency control, ultra-low frequency oscillation (ULFO).**

I. Introduction

In RECENT years, renewable energy has developed rapidly in the world. The multienergy complementary system can take advantage of the combination of different resources to promote the consumption of renewable energy [1]. The hydro-photovoltaic (PV) integrated system is a common form of multienergy complementary systems [2]. Through the complementarity of hydropower and PV, the volatility and schedulability of the overall system output power can be reduced and increased, respectively. As a result, the consumption capability of PV can be improved.

However, in a system with a high proportion of hydropower, the "water hammer effect" of the hydropower generator and an improper setting of its governor parameters will impose negative damping to the system, resulting in ultra-low frequency oscillations (ULFOs) with oscillation frequency lower than 0.1 Hz [3]. ULFO is different from the traditional low-frequency oscillation (LFO). Recently, ULFO has occurred in China, Türkiye, Colombia, and Northern Europe [4], and it seriously threatened the secure operation of the power system. So far, some research works have been carried out to analyze and solve the problem of ULFO.

For the oscillation mechanism and influencing factors analysis of ULFO, the damping torque and eigenvalue analysis method are two commonly used methods. Sun and Zhao [5] analyzed the damping torque of hydropower generators and revealed that the governor and turbine are prone to produce negative damping torque. Shi et al. [6] preformed eigenvalue analysis for a high proportion hydropower system and revealed a high participation of all governors on the ULFO.

Moreover, various approaches have been proposed in the literature to mitigate ULFOs. Since ULFO is caused by hydropower generators, these methods are mainly implemented on hydropower generators and can be categorized into three types.

1) *Retuning the governor parameters:* Generally, the ULFO can be mitigated by reducing the PID control parameters of governors [7], and this is the most studied method. Particle swarm optimization algorithm is used to optimize the governor parameters in [8]. However, the reduction of governor parameters can decrease the primary frequency regulation capability of hydropower generators.
2) *Power system stabilizer (PSS):* Conventional PSS is typically used to deal with the LFO problem, but they can also be effective against ULFOs. A PR-PSS algorithm to prevent ULFO is proposed in [9], and its parameter setting is adaptively updated by a deep reinforcement learning algorithm. In addition to the excitation system, PSS can also be implemented on the governor. Shi et al. [6] presented a design method for the governor PSS (GPSS) and validated its effectiveness.
3) *Quitting the hydropower governor:* The foundation of this method is to accurately locate the source of ULFO. Using an online damping torque estimation method [10] and energy flow method [11], generators with negative damping can be located. By quitting the governor of

Received 18 April 2024; revised 9 August 2024; accepted 7 September 2024. Date of publication 12 September 2024; date of current version 12 December 2024. This work was supported by the National Natural Science Foundation of China under Grant 52177066. Recommended for publication by Associate Editor M. S. ElMoursi. *(Corresponding author: Xiangyu Wu.)*

Sijia Wang, Yin Xu, Xiangyu Wu, and Jiaxuan Wang are with the School of Electrical Engineering, Beijing Jiaotong University, Beijing 100044, China (e-mail: wangsijia2020@bjtu.edu.cn; xuyin@bjtu.edu.cn; wuxiangyu@bjtu.edu.cn; 20121491@bjtu.edu.cn).

Gang Chen and Xueyang Zeng are with the Department of Power System Technology, State Grid Sichuan Electric Power Research Institute, Chengdu 610072, China (e-mail: cheng7216@sc.sgcc.com.cn; zengxy4411@sc.sgcc.com.cn).

Color versions of one or more figures in this article are available at https://doi.org/10.1109/TPEL.2024.3458910.

Digital Object Identifier 10.1109/TPEL.2024.3458910

these generators, ULFO can be suppressed. However, the frequency regulation function of governors is also lost after being quitted [12].

Inverter-based power sources, such as PV and battery energy storage, also have the potential to participate in mitigating ULFOs due to their active regulation capability. However, to the best of the authors' knowledge, how to use PV or battery energy storage to mitigate ULFO has been seldom studied. The existing research mainly focuses on utilizing PV [13], [14], [15] or battery energy storage [16], [17], [18], [19], [20] to suppress LFO or other kinds of oscillations. For example, Zhu et al. [16] presented an optimization approach for the control parameters of battery energy storage to improve the oscillation damping of power systems. Shi et al. [18] presented a robust control method of the energy storage system to effectively suppress LFO. A distributed control method based on multiagent deep reinforcement learning can dynamically modify the parameters of energy storage to suppress oscillations under different conditions [19].

For a hydro-PV integrated system, a system frequency response model can aid the design of ULFO damping controllers of PV. Although the system frequency response model for hydropower systems has been widely investigated, the frequency response model for hydro-PV integrated system has seldom been reported before.

Motivated by the aforementioned limitations, this article establishes a frequency response model of hydro-PV integrated systems and further presents a supplementary damping control method for PV plants to mitigate ULFOs. The contributions of this article are summarized as follows.

1) Unlike the traditional Phillips–Heffron model that considers grid-connected systems, this article establishes a frequency response model for islanded hydro-PV integrated systems, which is more suitable for analyzing ULFOs.
2) A supplementary damping controller is proposed for PV plants. Corresponding damping control parameters are designed based on our frequency response model theoretically.
3) The ULFO analysis and damping control method for multihydropower and multi-PV systems are furthermore provided. Specially,
   a) the damping torque theory is used for analyzing the ULFO mechanism of multihydropower and multi-PV systems;
   b) the frequency response model for multihydropower and multi-PV systems is provided;
   c) the method of how to use the frequency response model to calculate the eigenvalues of multihydropower and multi-PV systems is provided;
   d) the PV damping control method for multihydropower and multi-PV systems is proposed, and the damping control parameters of multiple PV plants are collaboratively designed.

Finally, the basic and supplementary control algorithm of PV is programmed into the digital signal processor (DSP), and a hardware platform based on RT-LAB and DSP controller is built. Time-domain simulation and experimental results validate the effectiveness of our proposed model and method for single-machine system and multihydropower and multi-PV systems.

The rest of this article is organized as follows. Section II analyzes the inadaptability of traditional Phillips–Heffron model. Section III establishes the frequency response model of islanded system. Section IV presents the supplementary damping control method of PV. Section V extends the proposed model and method to multihydropower and multi-PV systems. Sections V and VI provide the case study results based on time-domain simulations and experiments, respectively. Finally, Section VII concludes this article.

II. Damping Torque Analysis of Hydropower and Inadaptability Analysis for Phillips–Heffron Model

A. Damping Torque Analysis for Hydropower

The motion equation of the hydropower generator rotor is given by

$$T_J \frac{d\Delta\omega}{dt} = \Delta P_m - \Delta P_e - D\Delta\omega \tag{1}$$

where T_J is the inertia time constant of the synchronous generator, $\Delta\omega$ is the increment of the rotor speed, ΔP_{m} and ΔP_{e} are the increment of the mechanical power and electromagnetic power, respectively, and D is the damping coefficient. ΔP_{m} can be described as

$$\Delta P_m = -G_{\mathrm{gov}}(s)\, G_T(s)\, \Delta\omega \tag{2}$$

where $G_{\mathrm{gov}}(s)$ and $G_T(s)$ represent the governor model and turbine model, respectively. Detailed models are shown in (A1) and (A2) of Appendix A.

Based on the damping torque analysis method [21], through mathematical derivation, ΔP_{m} can be decomposed into

$$\Delta P_m = -D_m\Delta\omega - K_m\Delta\delta \tag{3}$$

where D_m and K_m are the damping torque and the synchronous torque of ΔP_{m} at the frequency ω_{d}, which can be calculated as

$$\begin{cases} D_m = Re\left(G_{\mathrm{gov}}(j\omega_d)\, G_T(j\omega_d)\right) \\ K_m = Im\left(G_{\mathrm{gov}}(j\omega_d)\, G_T(j\omega_d)\right). \end{cases} \tag{4}$$

Similarly, ΔP_e can also be decomposed into

$$\Delta P_e = D_e\Delta\omega + K_e\Delta\delta \tag{5}$$

where D_e and $\mathrm{K_e}$ are the damping torque and synchronous torque of ΔP_{e}, respectively.

According to (3) and (5), the motion equation of generator rotor can be rewritten as

$$T_J \frac{d\Delta\omega}{dt} = -\left(D_m + D_e + D\right)\Delta\omega - \left(K_m + K_e\right)\Delta\delta. \tag{6}$$

Fig. 1 shows the decomposition on the $\Delta\omega$–$\Delta\delta$ plane for the terms in the motion equation of hydropower generator rotors. The total damping torque of the system is $D_\Sigma = D_m + D_e + D$. A bigger D_Σ indicates a higher system damping. The system stability condition is that $D_\Sigma > 0$. Therefore, it can be deduced that 1) when $D_{\mathrm{m}} < 0$, ΔP_{m} provides negative damping, and 2) when $D_{\mathrm{e}} > 0$, ΔP_{e} provides positive damping. For the case in Fig. 1, D_Σ is less than 0 ($D_\Sigma < 0$) due to the large negative damping torque provided by the governor $G_{\mathrm{gov}}(s)$ and turbine $G_T(s)$ terms in ΔP_m, indicating an unstable system.

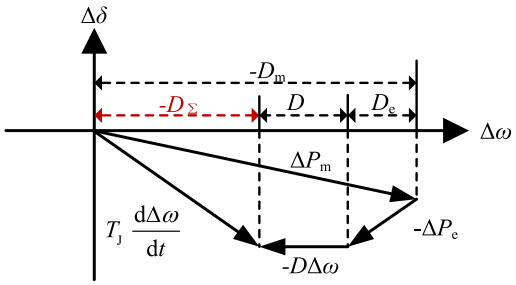

Fig. 1. Decomposition on the $\Delta\omega$–$\Delta\delta$ plane for the terms in the motion equation of generator rotor.

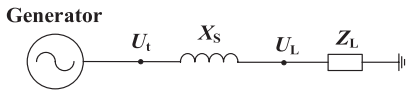

Fig. 2. Islanded single-machine system for the analysis of ULFO.

Therefore, the ULFO is mainly caused by the governor and turbine of hydropower generator.

B. Inadaptability Analysis for Phillips–Heffron Model

From (6), D_e is an important term in D_Σ. To calculate D_e, we need to accurately express ΔP_e. In the existing analysis for ULFOs [6], [22], ΔP_e is described based on the Phillips–Heffron model [21] shown in Appendix A. The Phillips–Heffron model is derived on the basis of the single-machine infinite-bus system. However, ULFO usually occurs in islanded hydropower systems [6]. Therefore, the Phillips–Heffron model is not suitable for describing ΔP_e. In sum, the expression of ΔP_e in the islanded hydropower systems needs to be formulated to obtain the corresponding frequency response model for analyzing ULFO.

III. Frequency Response Model for Islanded Hydropower System

The expression of ΔP_e and corresponding frequency response model for the islanded hydropower system is formulated in this section. Fig. 2 shows the studied islanded single-machine system composed of a hydropower generator and a constant impedance load, where U_t is the terminal voltage of generator, X_s is the impedance of the transmission line, Z_L is the impedance of the load, and U_L is the voltage on the load.

The expressions of P_e, E_q, U_{Lq} and U_{Ld} are provided in (A3) and (A4) of Appendix A. According to (A3) and (A4), the increments of i_d and i_q can be derived as

$$\begin{cases} \Delta i_d = \frac{(X_q+X_s)}{(X'_d+X_s)(X_q+X_s)-Z_L^2}\Delta E'_q \\ \Delta i_q = \frac{Z_L}{(X'_d+X_s)(X_q+X_s)-Z_L^2}\Delta E'_q. \end{cases} \tag{7}$$

Linearizing (A3) and then combing (7) and the linearized result, ΔP_e can be expressed as

$$\Delta P_e = \frac{2E'_{q0}Z_L\left[(X_q+X_s)^2-Z_L^2\right]}{\left[(X'_d+X_s)(X_q+X_s)-Z_L^2\right]^2}\Delta E'_q \tag{8}$$

where E'_{q0} is the equilibrium point value of E'_q.

To further express $\Delta E'_q$, the dynamic equation of the exciter is modeled as

$$T'_{d0}\frac{dE'_q}{dt} = E_{fd} - E_q \tag{9}$$

where T'_{d0} is the excitation time constant, and E_{fd} is the exciting voltage.

According to (A3), (7), and (9), $\Delta E'_q$ can be expressed in terms of ΔE_{fd}, given by

$$\left[T'_{d0}s + 1 + \frac{(X_q - X'_d)(X_q+X_s)}{(X'_d+X_s)(X_q+X_s)-Z_L^2}\right]\Delta E'_q = \Delta E_{fd}. \tag{10}$$

The expression of ΔE_{fd} can be obtained according to the structure of the excitation control system, i.e.,

$$E_{fd} = \frac{K_A}{1+sT_E}(U_{\text{ref}} - U_t + U_{\text{PSS}}) \tag{11}$$

where K_A and T_E are the gain coefficient and time constant of the excitation control system, U_{ref} is the voltage reference value, and U_{PSS} is the output signal of PSS.

Linearizing (11) yields

$$\Delta E_{fd} = \frac{K_A}{1+sT_E}(\Delta U_{\text{PSS}} - \Delta U_t). \tag{12}$$

ΔU_{PSS} can be expressed as

$$\begin{cases} \Delta U_{PSS} = G_{\text{PSS}}(s)\Delta\omega \\ G_{\text{PSS}}(s) = \frac{K_d s}{1+T_d s}\left(\frac{1+T_1 s}{1+T_2 s}\right)^2 \end{cases} \tag{13}$$

where $G_{\text{PSS}}(s)$ is the transfer function of PSS, K_d is the PSS gain, T_d is the washout time constant, T_1 is the lead time constant, and T_2 is the lag time constant.

U_t can be described as (A5) of Appendix A. From (A5) and the circuit relationship, we have

$$\begin{cases} \Delta U_t = \frac{U_{td0}}{U_{t0}}\Delta U_{td} + \frac{U_{tq0}}{U_{t0}}\Delta U_{tq} \\ \Delta U_{td} = (X_s + Z_L)\Delta i_d \\ \Delta U_{tq} = -(X_s + Z_L)\Delta i_q \end{cases} \tag{14}$$

where U_{td0}, U_{tq0}, and U_{t0} are the equilibrium point values of U_{td}, U_{tq}, and U_t, respectively.

Then, a detailed expression of ΔU_{t} can be obtained by substituting (7) into (14), i.e.,

$$\Delta U_t = \frac{(X_s+Z_L)\left[U_{td0}(X_q+X_s) - U_{tq0}Z_L\right]}{U_{t0}\left[(X'_d+X_s)(X_q+X_s)-Z_L^2\right]}\Delta E'_q. \tag{15}$$

Finally, the complete expression of ΔP_e can be obtained by combining (8), (10), (12), (13), and (15), i.e.,

$$\begin{cases} \Delta P_e = G_e(s)G_{PSS}(s)\Delta\omega \\ G_e(s) = \frac{A\left(T'_{d0}s+1+B\right)(1+sT_E)}{\left(T'_{d0}s+1+B\right)(1+sT_E)+K_A C} \end{cases} \tag{16}$$

where the expressions of A, B, and C are shown in the following:

$$\begin{cases} A = \frac{2E'_{q0}Z_L\left[(X_q+X_s)^2-Z_L^2\right]}{\left[(X'_d+X_s)(X_q+X_s)-Z_L^2\right]^2} \\ B = \frac{(X_q-X'_d)(X_q+X_s)}{(X'_d+X_s)(X_q+X_s)-Z_L^2} \\ C = \frac{(X_s+Z_L)[U_{td0}(X_q+X_s)-U_{tq0}Z_L]}{U_{t0}\left[(X'_d+X_s)(X_q+X_s)-Z_L^2\right]}. \end{cases} \tag{17}$$

From (16), the expression of ΔP_e in the islanded system is totally different from that in the Phillips–Heffron model of Fig. 18. Based on (16), the structure diagram of the frequency

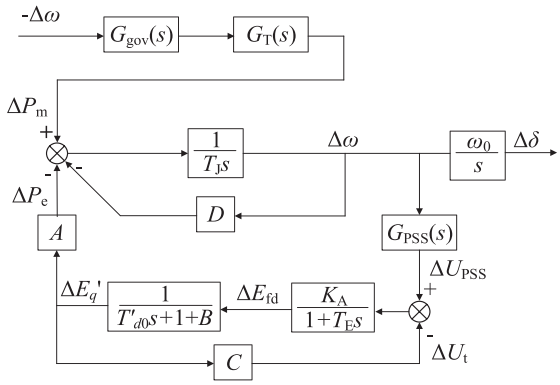

Fig. 3. Proposed islanded frequency response model.

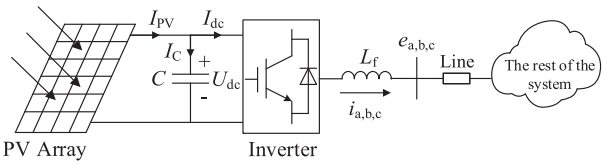

Fig. 4. Structure of a PV plant connected to the power system.

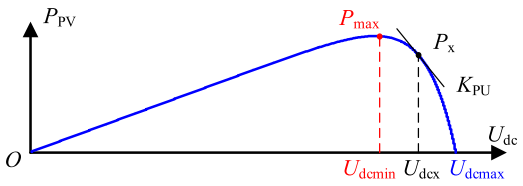

Fig. 5. Relationship between P_{PV} and U_{dc} of the PV array.

response model for the islanded hydropower system can be described in Fig. 3.

IV. Supplementary Damping Control Method of PV

Based on the islanded frequency response model formulated in Section III, this section further formulates the frequency response model of hydro-PV integrated system (see Section IV-C) and then proposes a supplementary damping control method for PV to mitigate ULFOs (see Section IV-D). To be the basis, the PV array model and basic control methods of PV inverters will be illustrated first in Sections IV-A and B, respectively.

A. PV Array Model

The PV plant model mainly includes the PV array, the inverter, and the controllers. Fig. 4 shows the structure of a PV plant connected to the power system.

In this article, the approximate engineering equivalent model of the PV cell is used [23]. Detailed model is shown in Appendix A. Then, the output power P_{PV} of the PV array is given by

$$P_{PV} = U_{dc} I_{PV} = U_{dc} m I_{sc} \left[1 - C_1 \left(e^{\frac{U_{dc}}{nC_2 U_{oc}}} - 1\right)\right]. \quad (18)$$

From (18), the relationship between P_{PV} and U_{dc} (P–U characteristic) is shown in Fig. 5. Due to the P–U characteristics, P_{PV} can be regulated by changing U_{dc}. Therefore, when U_{dc} is controlled to be changed according to the system frequency, P_{PV} is then correspondingly changed. Under this control mechanism, PV is potential to provide positive damping torque for ULFO and thus participates in mitigating ULFO. Detailed control mechanism and damping controller design method will be illustrated in Sections IV-C and D.

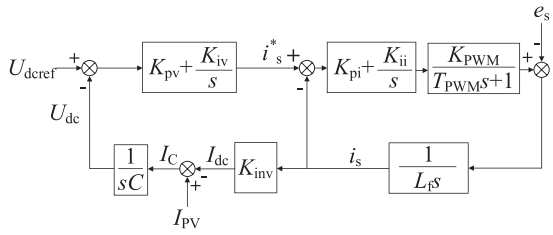

Fig. 6. Basic control structure of PV inverter.

Moreover, to have a better regulation capability for PV, a certain proportion of the PV output power away from the maximum power point (P_{max}) can be reserved. For example, the PV array can work at the point (U_{dcx}, P_x) in Fig. 5.

By linearizing (28) at point (U_{dcx}, P_x), we have

$$\begin{cases} \Delta P_{PV} = K_{PU} \Delta U_{dc} \\ K_{PU} = m I_{sc} \left[1 - C_1 \left(e^{\frac{U_{dcx}}{nC_2 U_{oc}}} - 1 + U_{dcx} \frac{e^{\frac{U_{dcx}}{nC_2 U_{oc}}}}{nC_2 U_{oc}}\right)\right] \end{cases} \quad (19)$$

where K_{PU} is the value of the slope corresponding to point (U_{dcx}, P_x).

B. Basic Control Method of PV Inverter

The basic control method of PV inverters is shown in Fig. 6, where U_{dcref} is the reference value of U_{dc}, K_{inv} is the equivalent gain of the inverter, K_{PWM} is the equivalent gain of the PWM modulation, K_{pv} and K_{iv} are the proportional and integral coefficients of the outer dc voltage loop, K_{pi} and K_{ii} are the proportional and integral coefficients of the inner current loop, L_f and C are the inductor and capacitor in Fig. 4. From Fig. 6, the dc voltage controller regulates U_{dc} to its reference value U_{dcref}. The current controller realizes the control of the inverter actual output current i_s to its reference value i_s^*.

With U_{dcref} as the input and U_{dc} as the output, the transfer function $G_{PV}(s)$ of the PV inverter controller can be derived as [24]

$$\begin{cases} G_{PV}(s) = \frac{\Delta U_{dc}}{\Delta U_{dcref}} = \frac{A_{PV}(s)}{B_{PV}(s)} \\ A_{PV}(s) = K_{inv} K_{pi} K_{pv} K_{PWM} s^2 + K_{inv} K_{ii} K_{pv} K_{PWM} s \\ \qquad + K_{inv} K_{ii} K_{iv} K_{PWM} \\ B_{PV}(s) = C L_f T_{PWM} s^5 + C L_f s^4 + C K_{pi} K_{PWM} s^3 \\ \qquad + (C K_{ii} K_{PWM} + K_{inv} K_{pi} K_{pv} K_{PWM}) s^2 \\ \qquad + (K_{inv} K_{ii} K_{pv} K_{PWM} + K_{inv} K_{ii} K_{iv} K_{PWM}) s \\ \qquad + K_{inv} K_{pi} K_{iv} K_{PWM}. \end{cases} \quad (20)$$

According to (20), the amplitude and phase of $G_{PV}(s)$ can be calculated, which can be used to design the supplementary controller and control parameters.

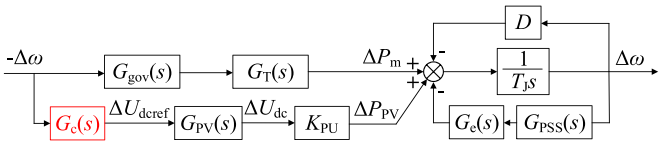

Fig. 7. Frequency response model for hydro-PV integrated system.

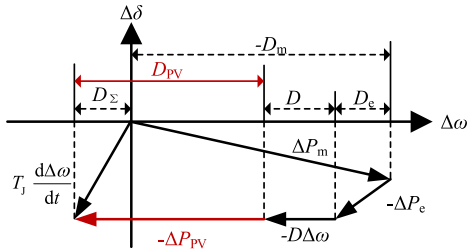

Fig. 8. Decomposition on the $\Delta\omega$–$\Delta\delta$ plane for the terms in (21).

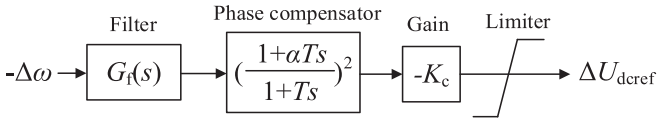

Fig. 9. PV supplementary damping controller.

C. Frequency Response Model of Hydro-PV Integrated System

For a single-hydropower and single-PV system, (1) can be modified as

$$T_J \frac{d\Delta\omega}{dt} = \Delta P_m - \Delta P_e - D\Delta\omega + \Delta P_{\mathrm{PV}}. \tag{21}$$

Considering (19), (20), (21), and Fig. 3, the frequency response model of the hydro-PV integrated system is shown in Fig. 7. Note that in Fig. 7, the lower part in Fig. 3 is compactly expressed as $G_e(s)$ in (21). In Fig. 7, $G_c(s)$ represents the supplementary damping controller of PV, which regulates $\Delta U_{\mathrm{dcref}}$ according to $\Delta\omega$. By adding $G_c(s)$, the PV output power ΔP_{PV} can respond to the system frequency change, i.e., ΔP_{PV} can be expressed as

$$\Delta P_{\mathrm{PV}} = K_{\mathrm{PU}} G_{\mathrm{PV}}(s)\, G_c(s)\, \Delta\omega. \tag{22}$$

The decomposition on the $\Delta\omega$-$\Delta\delta$ plane for the terms in (21) is shown in Fig. 8. The difference between Figs. 1 and 8 is the introduction of ΔP_{PV}. Based on (22), ΔP_{PV} can be expressed as $\Delta P_{\mathrm{PV}} = D_{\mathrm{PV}}\Delta\omega$. The detailed expression of D_{PV} will be given in Section IV-D. From Fig. 8, after introducing D_{PV}, we have $D_\Sigma = D_m + D_e + D + D_{\mathrm{PV}}$ and $D_\Sigma > 0$. Therefore, the PV can provide positive damping torque for ULFO, and the system becomes stable by adding the PV supplementary damping controller.

D. Supplementary Damping Control Method of PV

This section illustrates the design method for the supplementary damping controller $G_c(s)$. $G_c(s)$ consists of four parts: filter, phase compensator, gain, and limiter, as shown in (23) and Fig. 9. The design method of each part is provided as follows:

$$G_c(s) = -K_c G_f(s) \left(\frac{1+\alpha T s}{1+Ts}\right)^2. \tag{23}$$

1) *Filter:* The frequency signal $\Delta\omega$ is filtered to obtain ultra-low frequency components to avoid adverse effects of the damping controller on other frequency bands. The filter is a second-order band-pass filter, given by

$$G_f(s) = \frac{\frac{\omega_0}{Q}s}{s^2 + \frac{\omega_0}{Q}s + \omega_0^2} \tag{24}$$

where ω_0 is the center frequency of the ultra-low frequency band, and Q is the quality factor. The calculation methods of ω_0 and Q are shown in (25). Since the frequency range of ULFO is generally 0.01–0.1 Hz, the upper and lower frequency limits are selected as $f_{\min} = 0.01$ Hz and $f_{\max} = 0.1$ Hz, respectively

$$\begin{cases} \omega_0 = 2\pi f_0 \\ Q = \frac{f_0}{f_{\max} - f_{\min}} \\ f_0 = \sqrt{f_{\max} f_{\min}}. \end{cases} \tag{25}$$

2) *Phase compensator:* From Fig. 8, when ΔP_{PV} is in the opposite direction of $\Delta\omega$, the damping provided by PV is the largest. To realize this case, from (22), the phase compensation in $G_c(s)$ needs to generate a leading phase to offset the lagging phase of $G_{\mathrm{PV}}(s)$. By substituting $s = j\omega_0$ into (20), the lagging phase of the PV controller at ω_0, denoted as ϕ_x, can be obtained, given by

$$\phi_x = \arccos\left(\frac{Re\left(G_{\mathrm{PV}}\left(j\omega_0\right)\right)}{\left|G_{\mathrm{PV}}\left(j\omega_0\right)\right|}\right) \tag{26}$$

Considering that the leading phase provided by the phase compensation component is also ϕ_x, the corresponding parameters α and T can be calculated as

$$\begin{cases} \alpha = \frac{1+\sin\frac{\phi_x}{2}}{1-\sin\frac{\phi_x}{2}} \\ T = \frac{1}{\sqrt{\alpha}\omega_0}. \end{cases} \tag{27}$$

3) *Gain K_c:* From Fig. 8, D_{PV} is the projection component of ΔP_{PV} on $\Delta\omega$ axis. Therefore, from (22), we can derive that

$$D_{\mathrm{PV}} = K_{\mathrm{PU}} \left|G_c\left(j\omega_0\right) G_{\mathrm{PV}}\left(j\omega_0\right)\right| \cos\left(\phi_{G_c} + \phi_x\right) \tag{28}$$

where ϕ_{G_c} is the phases of $G_c(j\omega_0)$.

Since 1) the amplitude of the dc voltage controller of PV is usually designed to be 1, 2) the magnitude of filter and phase compensation in $G_c(s)$ is designed as 1 at ω_0, and 3) ϕ_{G_c} has completely offset ϕ_x based on the aforementioned design, we know

$$\begin{cases} \left|G_{\mathrm{PV}}\left(j\omega_0\right)\right| = 1 \\ \left|G_c\left(j\omega_0\right)\right| = K_c \\ \phi_{G_c} + \phi_{G_{\mathrm{PV}}} = 0. \end{cases} \tag{29}$$

Based on (29), (28) can be rewritten as

$$D_{\mathrm{PV}} = K_{\mathrm{PU}} K_c. \tag{30}$$

Moreover, based on (3), (5), and (21), it can be derived that

$$T_J \frac{d\Delta\omega}{dt} = -\left(D_m + D_e + D + D_{\mathrm{PV}}\right)\Delta\omega - \left(K_m + K_e\right)\Delta\delta. \tag{31}$$

Substituting $\Delta\delta = \frac{\omega_n}{s}\Delta\omega$ into (31) and rearranging the substituted results, we have

$$T_J s^2 = -\left(D_m + D_e + D + D_{\mathrm{PV}}\right)s - \left(K_m + K_e\right)\omega_n \tag{32}$$

where ω_n is the rated angular frequency of the system.

The system damping ratio ξ can then be calculated according to (32), given by

$$\xi = \frac{D_m + D_e + D + D_{\mathrm{PV}}}{2\sqrt{T_J \omega_n \left(K_m + K_e\right)}}. \tag{33}$$

Therefore, once a desired system damping ratio ξ_0 is predetermined in the design process, D_{PV} can be calculated as

$$D_{\mathrm{PV}} = 2\xi_0 \sqrt{T_J \omega_n \left(K_m + K_e\right)} - \left(D_m + D_e + D\right). \tag{34}$$

Finally, according to (30) and (34), K_c can be obtained as

$$K_c = \frac{2\xi_0 \sqrt{T_J \omega_n \left(K_m + K_e\right)} - \left(D_m + D_e + D\right)}{K_{\mathrm{PU}}}. \tag{35}$$

4) *Limiter:* The function of the limiting is to make the PV array work on the right-hand side of the maximum power point. The limiting parameters U_{dcmin} and U_{dcmax} can be obtained according to the P–U characteristics shown in Fig. 5.

V. ULFO Analysis and Supplementary Damping Control for Multihydropower and Multi-PV Systems

The study system in the previous section is a single-hydropower and single-PV system. This section further considers the multihydropower and multi-PV system, and presents the corresponding 1) unified frequency response model, 2) supplementary damping control design method, 3) ULFO mechanism analysis method based on the damping torque theory, and 4) eigenvalue calculation method based on the unified frequency response model.

A. Unified Frequency Response Model for Multihydropower and Multi-PV System

When ULFO occurs, the speeds of different generators and the frequencies of different buses have the same amplitude and phase, i.e., the speeds and frequencies are unified [25]. Therefore, the unified frequency response model was proposed to model the frequency response characteristic for multihydropower systems. This section extends the unified frequency response model to further consider multi-PV. The difficulties are 1) how to introduce the total PV output power into the rotor motion equation of each hydropower generator, and 2) how to aggregate the individual rotor motion equations containing the PV output power.

Assume that the number of hydropower and PV in the system are N and M, respectively. Based on the fact that $\Delta\omega$ of each generator is the same during ULFO, the linearized generator rotor motion equation for the ith generator is given by

$$T_{Ji}\frac{d\Delta\omega}{dt} = \Delta P_{mi} - \Delta P_{ei} - D_i\Delta\omega. \tag{36}$$

It should be noted that $\Delta P_{\mathrm{m}i}$ and $\Delta P_{\mathrm{e}i}$ are per-unit values. Define K_i as

$$K_i = \frac{S_i}{S_\Sigma} \tag{37}$$

where S_i is the capacity of the ith generator, and S_Σ is the sum of S_i of all generators.

After considering PV and transforming PV output power to per-unit value, (36) can be rewritten as

$$T_{Ji}\frac{d\Delta\omega}{dt} = \Delta P_{mi} - \Delta P_{ei} - D_i\Delta\omega + \frac{K_i}{S_i}\sum_{j=1}^{M}\Delta P'_{\mathrm{PV}j} \tag{38}$$

where S_i is used for per-unit value transformation, $\Delta P'_{\mathrm{PV}j}$ is the actual value for the output power of jth PV, and $K_i\sum_{j=1}^{M}\Delta P'_{\mathrm{PV}j}$ represents the portion of all the PV output power allocated to the ith generator.

Substituting (37) into (38) and multiplying both sides by K_i yield

$$K_iT_{Ji}\frac{d\Delta\omega}{dt} = K_i\Delta P_{mi} - K_i\Delta P_{ei} - K_iD_i\Delta\omega + \frac{K_i}{S_\Sigma}\sum_{j=1}^{M}\Delta P'_{\mathrm{PV}j}. \tag{39}$$

By adding (39) of all the hydropower generators, we have

$$\sum_{i=1}^{N}K_iT_{Ji}\frac{d\Delta\omega}{dt} = \sum_{i=1}^{N}\left(K_i\Delta P_{mi} - K_i\Delta P_{ei} - K_iD_i\Delta\omega\right) + \sum_{i=1}^{N}\left(\frac{K_i}{S_\Sigma}\sum_{j=1}^{M}\Delta P'_{\mathrm{PV}j}\right). \tag{40}$$

From (37), we have $\sum_{i=1}^{N}K_i = 1$. Considering $\sum_{i=1}^{N}K_i = 1$, (40) can be transformed to

$$\sum_{i=1}^{N}K_iT_{Ji}\frac{d\Delta\omega}{dt} = \sum_{i=1}^{N}\left(K_i\Delta P_{mi} - K_i\Delta P_{ei} - K_iD_i\Delta\omega\right) + \frac{1}{S_\Sigma}\sum_{j=1}^{M}\Delta P'_{\mathrm{PV}j} \tag{41}$$

Equation (41) is the constructed aggregated rotor motion equation for the multihydropower and multi-PV system. For the ith hydropower, we have

$$\begin{cases}\Delta P_{ei} = G_{ei}\left(s\right)G_{\mathrm{PSS}i}\left(s\right)\Delta\omega \\ \Delta P_{mi} = -G_{\mathrm{gov}i}\left(s\right)G_{Ti}\left(s\right)\Delta\omega\end{cases} \tag{42}$$

For the jth PV, we have

$$\Delta P'_{\mathrm{PV}j} = K_{\mathrm{PU}j}G_{\mathrm{PV}j}\left(s\right)G_{cj}\left(s\right)\Delta\omega \tag{43}$$

where $G_{cj}(s)$ is the transfer function for the supplementary damping controller of the jth PV.

Based on (41)–(43) and Fig. 7, the unified frequency response model for the multihydropower and multi-PV system can be obtained, as shown in Fig. 10.

Remark 1: For the low- LFO, the frequencies of different nodes in the system are different, so the interactions among multimachines need to be modeled due to their different internal dynamics. However, for ultra- ULFO, the frequencies of each generator are the same during ULFO [8]. Therefore, the multimachines do not exhibit interactions in terms of frequency during ULFO. Based on this characteristic, a unified frequency can be used to describe the system frequency [25]. On this basis, a unified frequency response model is proposed for multihydropower and multi-PV systems in this article.

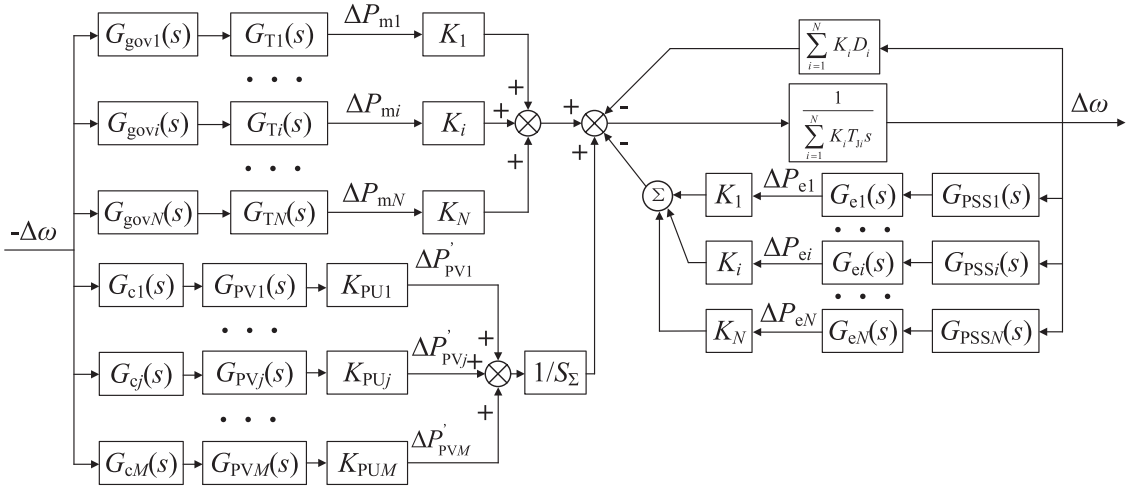

Fig. 10. Unified frequency response model of the multihydropower and multi-PV system.

B. Supplementary Damping Control Design Method for Multi-PV

For multimachine systems, $G_{cj}(s)$is also composed of filtering, phase compensation, gain, and limiting. The design method for filtering, phase compensation, and limiting is the same with that of the single-hydropower and single-PV system. However, the calculation equation for gains K_{cj} in $G_{cj}(s)$ is different, which will be presented in the following.

For ΔP_{mi} and ΔP_{ei}, they can also be decomposed into

$$\begin{cases} \Delta P_{mi} = -D_{mi}\Delta\omega - K_{mi}\Delta\delta \\ \Delta P_{ei} = D_{ei}\Delta\omega + K_{ei}\Delta\delta. \end{cases} \tag{44}$$

For $\Delta P'_{\mathrm{PV}j}$, based on Section IV, it can be expressed as

$$\Delta P'_{\mathrm{PV}j} = D_{\mathrm{PV}j}\Delta\omega \tag{45}$$

$$D_{\mathrm{PV}j} = K_{\mathrm{PU}j}K_{cj} \tag{46}$$

where $D_{\mathrm{PV}j}$ is the damping torque provided by the *j*th PV.

Substituting (43), (44), and $\Delta\delta = \frac{\omega_n}{s}\Delta\omega$ into (41) and rearranging the substituted results, it can be derived that

$$\sum_{i=1}^{N} K_i T_{Ji} s^2 = -\sum_{i=1}^{N} K_i \left(D_{mi} + D_{ei} + D_i\right) s - \frac{\sum_{j=1}^{M} D_{\mathrm{PV}j}}{S_\Sigma} s - \sum_{i=1}^{N} K_i \omega_n \left(K_{mi} + K_{ei}\right). \tag{47}$$

Therefore, the damping ratio ξ_{mul} of the multimachine system can be calculated according to (47), given by

$$\xi_{\mathrm{mul}} = \frac{\sum_{i=1}^{N} K_i \left(D_{mi} + D_{ei} + D_i\right) + \frac{\sum_{j=1}^{M} D_{\mathrm{PV}j}}{S_\Sigma}}{2\sqrt{\omega_n \sum_{i=1}^{N} K_i T_{Ji} \sum_{i=1}^{N} K_i \left(K_{mi} + K_{ei}\right)}} \tag{48}$$

For a desired ξ_{mul0}, $\sum_{j=1}^{M} D_{\mathrm{PV}j}$ can be calculated from (48). For the calculation of $D_{\mathrm{PV}j}$ from $\sum_{j=1}^{M} D_{\mathrm{PV}j}$, it is reasonable that a PV with a larger capacity should correspondingly provide a larger damping torque. $D_{\mathrm{PV}j}$ is allocated according to the absolute slopes of its operating points on its *P*–*U* characteristic, i.e.,

$$D_{\mathrm{PV}j} = \frac{K_{PUj}}{\sum_{j=1}^{M} K_{PUj}} \sum_{j=1}^{M} D_{\mathrm{PV}j}. \tag{49}$$

Finally, based on (47)–(49), K_{cj} of each PV can be calculated as

$$K_{cj} = \frac{2S_\Sigma \xi_{\mathrm{mul0}} \sqrt{\omega_n \sum_{i=1}^{N} K_i T_{Ji} \sum_{i=1}^{N} K_i \left(K_{mi} + K_{ei}\right)}}{\sum_{j=1}^{M} K_{\mathrm{PU}j}} - \frac{S_\Sigma \sum_{i=1}^{N} K_i \left(D_{mi} + D_{ei} + D_i\right)}{\sum_{j=1}^{M} K_{\mathrm{PU}j}} \tag{50}$$

Remark 2: There are already some actual engineering projects of hydro-PV integrated system in the world, such as Yalong River Lianghekou and Xiaojin hydro-PV integrated system in Sichuan Province of China. With the increase of the PV's penetration level in the power grid, the demand for PV to participate in the power grid support and regulation is also increasing. Using PV plants to provide some auxiliary services to the system is a promising approach. Therefore, the existing PV plants that are already in the hydro-PV integrated system can be utilized to help damp the ULFO, which is a rational use of existing resources.

C. ULFO Mechanism Analysis Based on Damping Torque Theory and Eigenvalue Calculation Method Based on Unified Frequency Response Model

The damping torque analysis theory is innovatively used in this article to analyze the ULFO mechanism of multihydropower and multi-PV systems. Detailed analysis methods and results are given in Appendix C.

In addition, based on the constructed unified frequency response model, the eigenvalues of the multihydropower and multi-PV system are calculated and its stability characteristics are furthermore analyzed. Besides, the small-signal state-space modeling method, which is a well-known analytical tool/method for the analysis of small-signal stability problem, is also used to calculate the system eigenvalues. The eigenvalues obtained from

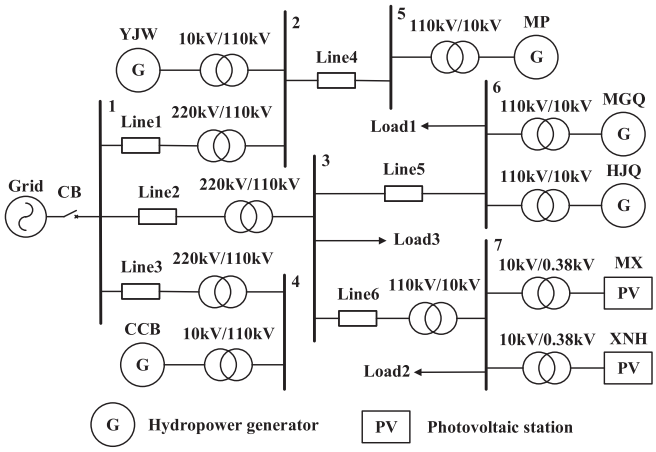

Fig. 11. Topology of hydro-PV integrated system in a county of Sichuan Province, China.

TABLE I
CAPACITIES OF POWER SOURCES

Name	Type	Capacity	Name	Type	Capacity
YJW	Hydro	75 MW	MGQ	Hydro	45 MW
MP	Hydro	55 MW	XNH	PV	10 MW
CCB	Hydro	65 MW	MX	PV	5 MW
HJQ	Hydro	140 MW			

TABLE II
SUPPLEMENTARY DAMPING CONTROL PARAMETERS

Parameters	XNH	MX
U_{dcx}	0.96 kV	0.96 kV
U_{dcmin}	0.871 kV	0.871 kV
U_{dcmax}	1.073 kV	1.073 kV
K_{PU}	27.6 MW/kV	13.8 MW/kV
ω_0	0.20 rad/s	0.20 rad/s
Q	0.35	0.35
α	1	1
T	5.03	5.03
K_c	3758	3758

the above two methods are compared to validate the accuracy of our frequency response model in calculating eigenvalues. Detailed analysis method and results are given in Appendix D.

VI. SIMULATION RESULTS

To validate the effectiveness of the proposed ULFO damping control method, time-domain simulation results are carried out based on an actual hydro-PV integrated system in a county of Sichuan Province, China.

A. Actual System of a County in Sichuan Province of China

The studied hydro-PV integrated system in a county of Sichuan Province of China is shown in Fig. 11. The system contains five hydropower generators and two PVs. Since ULFO usually occurs in an islanded system, the circuit breaker (CB) is set to be open. As a result, the system is disconnected from the external grids. Table I tabulates the capacities of power sources. Table II tabulates the parameters of the PV supplementary damping controllers, which can be calculated according to (25), (27), (50), and Fig. 5. Detailed parameters of hydropower generators, PV plants, lines, and loads are shown in Appendix B.

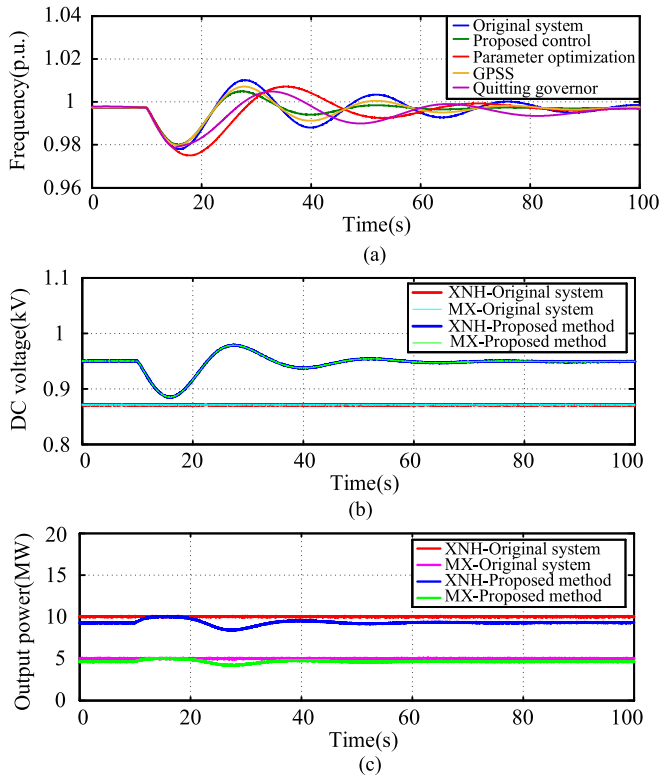

Fig. 12. Simulation results of Case1. (a) system frequency (b) PV DC voltage. (c) PV output power.

To verify the accuracy of the constructed frequency response model from the time domain and frequency domain, respectively, the comparison results of the frequency response curves and eigenvalues are provided in Appendix E.

In the following, Sections VI-B and C validate the effectiveness of the proposed ULFO damping control method in the cases of load change and instantaneous fault, respectively.

B. Validation of PV Supplementary Damping Control—Case 1: Load Change

The system load change is set as the disturbance in this case. Initially, Load 1 and Load 2 are connected, and Load 3 is disconnected. The total load in the system is 105 MW. At $t = 10$ s, Load 3 is connected. The total load in the system changes from 105 to 115 MW. Fig. 12 compares the simulation results of the original system without damping control, with the proposed supplementary damping control method of PV, with the governor parameter optimization method, with GPSS, and by quitting the hydropower governor. The responses of system frequency, dc voltage and output active power of XNH and MX PV are, respectively, shown in Fig. 12(a)–(c). The main idea of the governor parameter optimization method is to reduce the control gains of governors, which is the most widely used ULFO suppression method [7]. GPSS improves the negative damping of the hydropower governor by implementing PSS on the governor [6]. For the method of quitting the governor, the

TABLE III
RESULTS OF PRONY ANALYSIS

Name	Frequency/Hz	Damping ratio/%
Original system	0.0421	12.24
Governor parameter optimization	0.0284	24.12
Proposed method	0.0416	30.21

action time is $t = 15$ s, that is, 5 s after the oscillation occurs [12].

Fig. 12(a) indicates that the system occurs ULFOs after $t = 10$ s. All methods can mitigate the ULFO, but the proposed method exhibits the most desirable damping performance, which validates its superiority. Fig. 12(b) and (c) indicates that with our proposed method, the dc voltages of PV can respond to the change of system frequency, and the PV output power changes with the variation of dc voltage.

Remark 3: Our method is implemented on the PV side rather than the hydropower generator side. Therefore, we do not need to reduce the PID control parameters of governors or quit the governors of some hydropower generators. Hence, we can avoid the decrease of the primary frequency regulation ability of hydropower generators. In addition, compared with the solution of GPSS on the hydropower generator, we can avoid the additional wear of mechanical components.

In sum, the above simulation results show that our proposed method is effective to control the PV dc voltages to change their output power and thus participate in mitigating the ULFO.

Table III tabulates the results of Prony analysis of the ULFO signal shown in Fig. 13(a). Because the governor parameter optimization method is the most widely used, it is used to compare with the proposed method. It can be seen from Table III that the damping of original system is weak, but both the governor parameter optimization method and our proposed method can increase the damping ratio. Because the governor parameter optimization method needs to balance the ability of frequency regulation and ultra-low frequency damping [9], the effect of the proposed method is better.

A simulation comparison of the suppression effect of PV on the ULFO with or without reserving PV power is provided in Appendix F. The results show that when there is no reservation for PVs (MPPT mode), they can also suppress ULFO by reducing the output power. When 10% of PV maximum output power capability is reserved for control, the PVs can not only reduce but also increase their output power to obtain a better ULFO suppression effect.

C. Validation of PV Supplementary Damping Control—Case 2: Instantaneous Fault

The instantaneous fault is a common disturbance in power systems. Therefore, it is also used as a disturbance to test the proposed method. The total load in the system is 105 MW. At $t = 10$ s, a three-phase instantaneous fault with a duration of 0.1 s occurs at Bus 1 as a disturbance. Fig. 13 compares the simulation results of the original system without damping control, the traditional governor parameter optimization method, and our proposed supplementary damping control method of

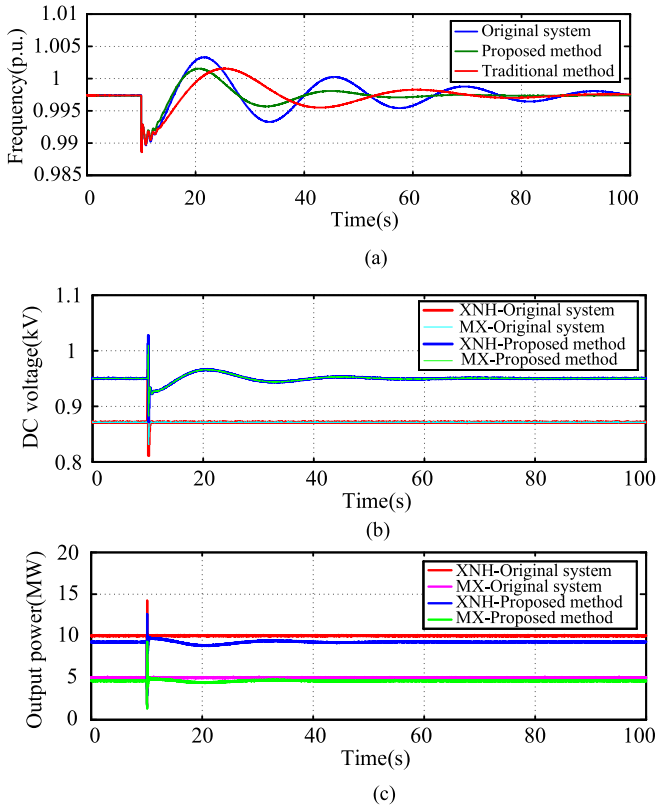

Fig. 13. Simulation results of Case2. (a) System frequency. (b) PV DC voltage. (c) PV output power.

TABLE IV
RESULTS OF PRONY ANALYSIS

Name	Frequency/Hz	Damping ratio/%
Original system	0.0414	11.83
Governor parameter optimization	0.0275	23.57
Proposed method	0.0411	30.05

PV. The responses of system frequency, dc voltage, and output active power of XNH and MX PV are, respectively, shown in Fig. 13(a)–(c).

Fig. 13(a) indicates that the system occurs ULFOs after $t = 10$ s. Both the proposed method and the governor parameter optimization method can mitigate the ULFO, but our proposed method exhibits a more desirable damping performance. Fig. 13(b) and (c) indicates that with our proposed method, the dc voltages of PV can respond to the change of system frequency, and the PV output power changes with the variation of dc voltage.

Table IV tabulates the results of Prony analysis of the ULFO signal shown in Fig. 13(a). The results of simulations and Prony analysis show that the proposed method is still effective in suppressing ULFO under the instantaneous fault, and the suppression effect is better than the governor parameter optimization.

The influence of intermittency characteristics of PV output power is analyzed by the simulation in Appendix G. The test results show that although the PV output power changes due to

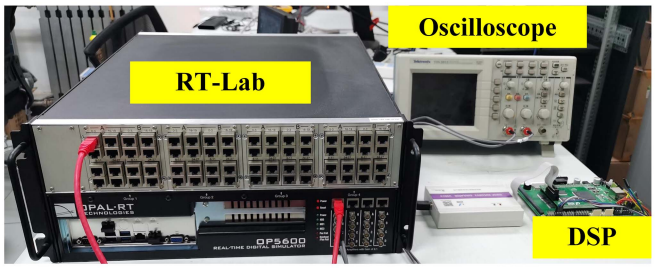

(a)

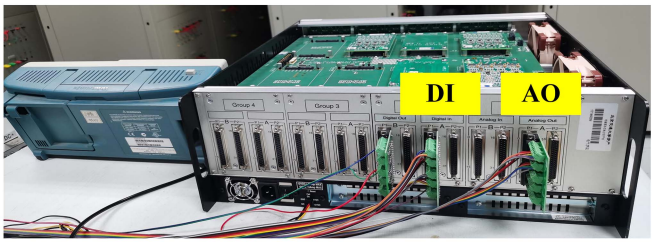

(b)

Fig. 14. Experimental platform. (a) RT-Lab, Oscilloscope, and DSP. (b) Connection between RT-Lab and DSP.

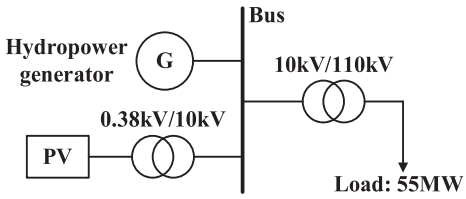

Fig. 15. Topology of the hydro-PV integrated system.

variation of sunlight intensity, the proposed PV supplementary controller can still have a desirable damping effect.

VII. Experimental Results

This section presents experimental results to validate the practical implementation feasibility of the proposed control.

A. Experiment Platform and Test System

Fig. 14 shows the hardware platform for the experimental study in the laboratory. The experimental setup mainly includes RT-LAB OP5600 and DSP controller. A simulation model of a hydro-PV integrated system is built in RT-LAB, including the models of hydropower generator, PV inverter, PV array, networks, and loads. The PV inverter control method is programmed in the DSP with type of TI TMS320F28377. The voltage and current are measured in RT-LAB and then transmitted to the DSP through AO interfaces. The DSP generates PWM signal and transmits it to RT-LAB through DI interfaces to control the PV inverter.

The topology of the test system is shown in Fig. 15. The parameters of hydropower generators and PV are given in Tables V and VI, respectively.

In the following, Section VII-B validates the accuracy of the constructed frequency response model. Section VI-C validates the effectiveness of the proposed ULFO damping control method in the case of the load change.

TABLE V
Parameters of Hydropower Generator

Parameter	Value	Parameter	Value	Parameter	Value
Capacity	100 MW	K_P	1.3	b_p	0.01
T_J	6 s	K_I	0.3	T_d	0.02
T_W	1.8 s	K_D	0		

TABLE VI
Parameters of PV Plant

Parameter	Value	Parameter	Value
Capacity	21 MW	C	1000 μF
K_{pv}	10	K_{PU}	58.98 MW/kV
K_{iv}	200	ω_0	0.20 rad/s
K_{pi}	10	Q	0.35
K_{ii}	25	T	5.03
K_{PWM}	1	K_c	594
T_{PWM}	0.01 s	U_{dcx}	960 V
L_f	0.04 mH	U_{dcmin}	871 V
K_{inv}	1	U_{dcmax}	1073 V

B. Accuracy Validation of the Constructed Frequency Response Model

Three parameter conditions of weak damping, strong damping, and negative damping of the studied system are set, respectively, for analysis, and Table XV in Appendix B shows these different parameters.

Based on the parameters in Table XV, the response of the system frequency is obtained from our proposed frequency response model and the experimental platform for the conditions of weak damping, strong damping, and negative damping. Fig. 16(a)–(c) shows the comparison results for the above three conditions, respectively. The small-signal disturbance is a load increase of 10 MW. From Fig. 16, the two responses are consistent with each other, thus validating the accuracy of our frequency response model.

Furthermore, based on the parameters in Table XV, the system eigenvalues are calculated from our proposed frequency response model for the conditions of weak damping, strong damping, and negative damping. The results of the ULFO mode in terms of the quantification criteria of oscillation frequency and damping ratio for the above three conditions are given in Table VII. Table VII also shows the Prony analysis results from the experimental results in Fig. 16. Table VII indicates that for each condition, there is little difference between the results of oscillation frequency and damping ratio from the frequency response model and those obtained by Prony analysis of the experimental results, validating the accuracy of the ULFO mode calculation results from our frequency response model.

C. Validation of PV Supplementary Damping Control

At $t = 10$ s, the total load in the system changes from 55 to 60 MW. Fig. 17(a) indicates that the ULFO occurs when the system is disturbed, and it takes a long time for the oscillations to decay. After introducing the PV supplementary damping control,

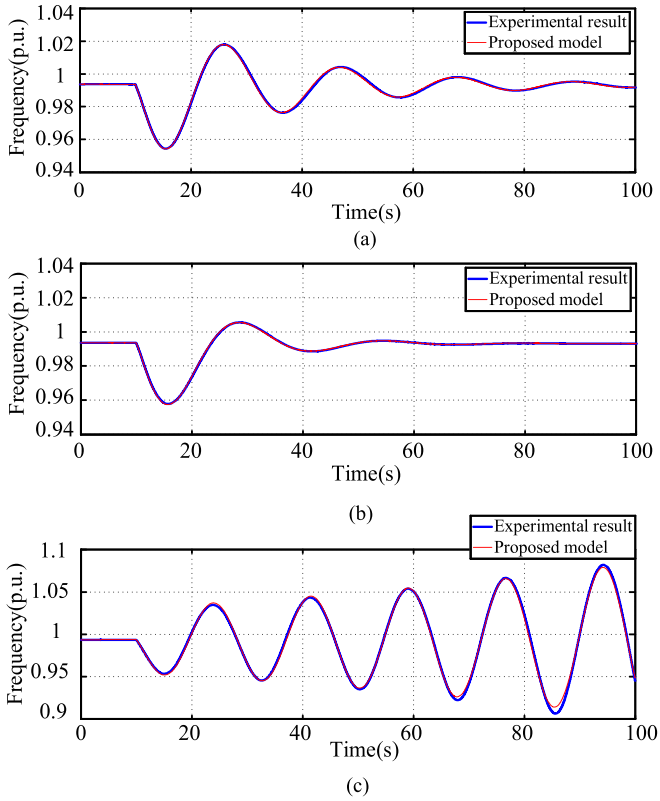

Fig. 16. Comparison results of the single-machine system: the response of the system frequency obtained from our proposed frequency response model and the experimental platform. (a) Weak damping. (b) Strong damping (c) Negative damping.

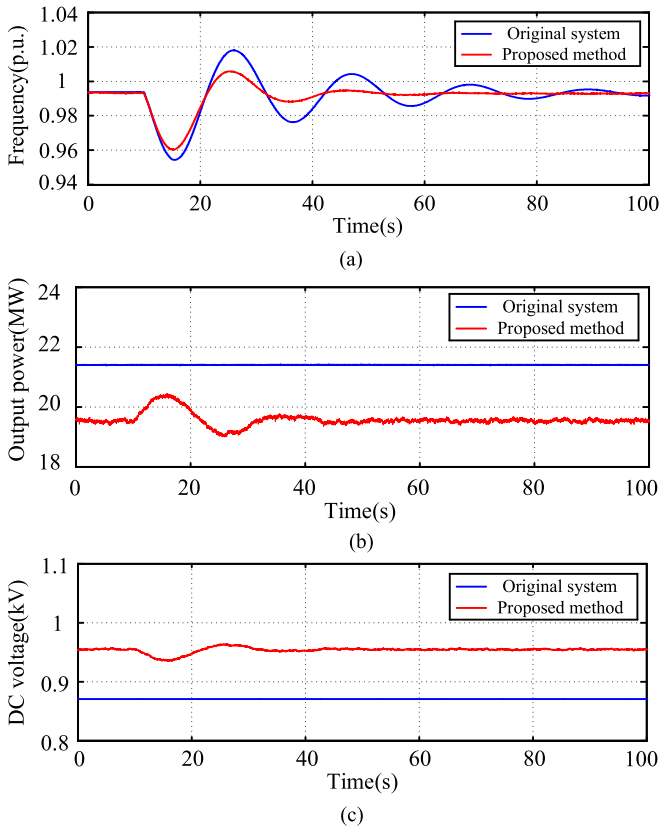

Fig. 17. Experimental results. (a) System frequency. (b) PV output power. (c) PV DC voltage.

TABLE VII
COMPARISON OF OSCILLATION FREQUENCY AND DAMPING RATIO OBTAINED FROM THE FREQUENCY RESPONSE MODEL AND PRONY ANALYSIS OF THE EXPERIMENTAL RESULTS

Condition	Proposed frequency response model		Prony analysis of the experimental result	
	Oscillation frequency	Damping ratio	Oscillation frequency	Damping ratio
Weak damping	0.0482 Hz	13.42%	0.0461 Hz	13.24%
Strong damping	0.039 Hz	31.53%	0.0384 Hz	30.12%
Negative damping	0.0569 Hz	–2.66%	0.0539Hz	–2.79%

In sum, the results of the constructed frequency response model can well match the experiments.

TABLE VIII
RESULTS OF PRONY ANALYSIS

Name	Frequency/Hz	Damping ratio/%
Original system	0.0461	13.24
Proposed method	0.0491	30

ULFO is effectively mitigated. As shown in Fig. 17(b) and (c), PV can actively change the output power by regulating the dc voltage according to the system frequency, thereby providing damping for the system and mitigating the ULFO.

Table VIII tabulates the results of Prony analysis of the ULFO signal shown in Fig. 17(a). It can be seen from Table VIII that the proposed control method significantly improves the damping of the system.

VIII. CONCLUSION

This article establishes a unified frequency response model for hydro-PV integrated systems, which is more suitable under the islanded condition, and further presents a supplementary damping control method for PV plants to mitigate ULFOs. The ULFO analysis and damping control method for multihydropower and multi-PV systems are furthermore provided. Damping torque analysis, eigenvalue analysis, time-domain simulation, and experimental results show the following.

1) The hydropower generator with the largest capacity and biggest water hammer effect time constant provides the largest negative damping torque, and the PV can provide positive damping torque in the ultra-low frequency band.
2) The system frequency response results from our frequency response model are consistent with those obtained from time-domain simulations and experiments, which validates our frequency response model in the time-domain.
3) The system eigenvalue results from our frequency response model are consistent with the results of time-domain simulations and experiments, which validates our frequency response model in the frequency-domain.

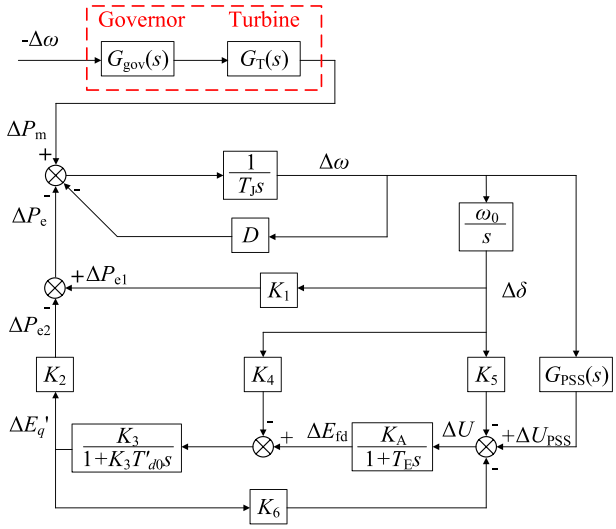

Fig. 18. Phillips–Heffron model including the governor, the turbine, and PSS.

4) Our PV supplementary controller exhibits better damping performance compared with the traditional methods and the case without our controller.

APPENDIX A

In this appendix, some models and equations are provided.

A. Transfer Function of Governor and Turbine

The transfer function of the governor $G_{\text{gov}}(s)$ is given by

$$G_{\text{gov}}(s) = \frac{K_D s^2 + K_P s + K_I}{b_P K_I + s} \frac{1}{1 + T_G s} \tag{A1}$$

where K_P, K_I, and K_D are the proportional, integral, and differential parameters, respectively. b_P is the adjustment coefficient. T_{G} is the time constant of the servo system.

The transfer function of the turbine $G_{\text{T}}(s)$ is given by

$$G_T(s) = \frac{1 - T_W s}{1 + 0.5 T_W s} \tag{A2}$$

where T_{W} is the water hammer time constant.

B. Phillips–Heffron Model

A lot of existing research works for ULFOs is based on the Phillips–Heffron model, as shown in Fig. 18, which is derived from the single-machine infinite-bus system.

C. Generator Equations

From basic generator equations, the generator electromagnetic power P_{e} and the q-axis equivalent voltage E_q are given by

$$\begin{cases} P_e = E_q i_q \\ E_q = E'_q + (X_q - X'_d)\, i_d \end{cases} \tag{A3}$$

where i_q and i_d are the q-axis and d-axis currents, X_q is the q-axis synchronous reactance of the stator, X'_d is the d-axis synchronous transient of the stator, and E'_q is the q-axis transient voltage of the generator.

Denote U_{Lq} and U_{Ld} as the q-axis and d-axis voltages of U_L, and we have

$$\begin{cases} E'_q - U_{Lq} = (X'_d + X_s)\, i_d \\ U_{Ld} = (X_q + X_s)\, i_q \\ U_{Lq} = Z_L i_d \\ U_{Ld} = -Z_L i_q. \end{cases} \tag{A4}$$

U_{t} can be described as

$$U_t = \sqrt{U_{td}^2 + U_{tq}^2} \tag{A5}$$

where U_{td} and U_{tq} are the d-axis and q-axis output voltages of U_{t}.

D. PV Array Model

The standard parameters of PV cell in the rated condition ($S_{\text{ref}} = 1000\,\text{W/m}^2$, $T_{\text{ref}} = 25\,^\circ\text{C}$) are denoted as the open-circuit voltage U_{ocref}, the short circuit current I_{scref}, the voltage of the maximum power point $U_{m\text{ref}}$ and the current of the maximum power point $I_{m\text{ref}}$. The values of PV cell parameters in other conditions can be obtained by

$$\begin{cases} T = T_{\text{air}} + kS \\ I_{\text{sc}} = I_{\text{scref}} \frac{S}{S_{\text{ref}}} \left[1 + \alpha (T - T_{\text{ref}})\right] \\ I_m = I_{m\text{ref}} \frac{S}{S_{\text{ref}}} \left[1 + \alpha (T - T_{\text{ref}})\right] \\ U_{\text{oc}} = U_{\text{ocref}} \left[1 - \gamma (T - T_{\text{ref}})\right] \ln\left[e + \beta \left(\frac{S}{S_{\text{ref}}} - 1\right)\right] \\ U_m = U_{m\text{ref}} \left[1 - \gamma (T - T_{\text{ref}})\right] \ln\left[e + \beta \left(\frac{S}{S_{\text{ref}}} - 1\right)\right] \end{cases} \tag{A6}$$

where T is the temperature of the PV cell, T_{air} is the air temperature, k is the temperature coefficient, and the compensation coefficients α, β, γ are 0.0025 °C, 0.5 m²/W, and 0.00288 °C, respectively.

Based on the PV cell model, the *U–I* equation of the PV array with n cells in series and m cells in parallel can be described as

$$I_{\text{PV}} = m I_{\text{sc}} \left[1 - C_1 \left(e^{\frac{U_{\text{dc}}}{n C_2 U_{\text{oc}}}} - 1\right)\right] \tag{A7}$$

where I_{PV} is the output current of the PV array, I_{sc} is the short circuit current, U_{dc} is the dc voltage of PV, U_{oc} is the open-circuit voltage, and the constants C_1 and C_2 are

$$\begin{cases} C_1 = (1 - I_m / I_{\text{sc}})\, e^{-\frac{U_m}{C_2 U_{\text{oc}}}} \\ C_2 = \frac{U_m / U_{\text{oc}} - 1}{\ln(1 - I_m / I_{\text{sc}})} \end{cases} \tag{A8}$$

where I_m and U_m are the voltage and current at the maximum power point.

APPENDIX B

In this appendix, some parameters used in this paper are provided.

The parameters of hydropower generators, PV plants, lines, and loads used in the actual hydro-PV integrated system of Section VI are shown in the Tables IX–XI, respectively.

Three parameter conditions of weak damping, strong damping, and negative damping of the studied system are set, respectively, for the system with five hydropower generators and 2 PV stations shown in Fig. 11, and Tables XII–XIV shows these different parameters.

TABLE IX
PARAMETERS OF HYDROPOWER GENERATORS

Generator	T_J	T_W	K_P	K_I	K_D	b_p	T_d	D
YJW	6.5 s	2 s	1.5	0.28	0	0.01	0.02 s	0
MP	5 s	1.8 s	1.8	0.3	0	0.01	0.02 s	0
CCB	6 s	2 s	1.5	0.28	0	0.01	0.02 s	0
HJQ	8 s	2.5 s	1.3	0.25	0	0.01	0.02 s	0
MGQ	4.5 s	1.8 s	1.8	0.3	0	0.01	0.02 s	0

TABLE X
PARAMETERS OF PV PLANTS

PV	K_{pv}	K_{iv}	K_{pi}	K_{ii}	K_{PWM}	T_{PWM}	L_f/mH	K_{inv}	C/μF
XNH	10	100	5	25	1	0.01	0.04	1	8000
MX	10	100	5	25	1	0.01	0.04	1	8000

TABLE XI
PARAMETERS OF LINES AND LOADS

Line and load	Value
Line1	0.0019+j0.0106 p.u.
Line2	0.0043+j0.03499 p.u.
Line3	0.0004+j0.0019 p.u.
Line4	0.0021+j0.0119 p.u.
Line5	0.0007+j0.0021 p.u.
Line6	0.0005+j0.0019 p.u.
Load1	25 MW
Load2	80 MW
Load3	10 MW

TABLE XII
PARAMETERS OF HYDROPOWER GENERATORS UNDER WEAK DAMPING CONDITION

Generator	T_J	T_W	K_P	K_I	b_p	T_d
YJW	6.5 s	1.8 s	1.2	0.3	0.01	0.02 s
MP	5 s	1.5 s	1.3	0.32	0.01	0.02 s
CCB	6 s	1.5 s	1.2	0.3	0.01	0.02 s
HJQ	8 s	2 s	1	0.28	0.01	0.02 s
MGQ	4.5 s	1.2 s	1.3	0.32	0.01	0.02 s

Three parameter conditions of weak damping, strong damping, and negative damping of the studied single-machine system of Fig. 16 are set, respectively, for analysis, and Table XV shows these different parameters.

TABLE XIII
PARAMETERS OF HYDROPOWER GENERATORS UNDER STRONG DAMPING CONDITION

Generator	T_J	T_W	K_P	K_I	b_p	T_d
YJW	6.5 s	1.8 s	1.28	0.23	0.01	0.02 s
MP	5 s	1.5 s	1.38	0.25	0.01	0.02 s
CCB	6 s	1.5 s	1.18	0.23	0.01	0.02 s
HJQ	8 s	2 s	1.08	0.21	0.01	0.02 s
MGQ	4.5 s	1.2 s	1.38	0.25	0.01	0.02 s

TABLE XIV
PARAMETERS OF HYDROPOWER GENERATORS UNDER NEGATIVE DAMPING CONDITION

Generator	T_J	T_W	K_P	K_I	b_p	T_d
YJW	6.5 s	1.8 s	1.2	0.42	0.01	0.02 s
MP	5 s	1.5 s	1.3	0.44	0.01	0.02 s
CCB	6 s	1.5 s	1.2	0.42	0.01	0.02 s
HJQ	8 s	2 s	1	0.4	0.01	0.02 s
MGQ	4.5 s	1.2 s	1.3	0.44	0.01	0.02 s

APPENDIX C

In this appendix, the damping torque analysis theory is innovatively used to analyze the ULFO mechanism of multihydropower and multi-PV systems. Detailed analysis methods and results are provided as follows.

A. Analysis for the System With Five Hydropower Generators

Based on the derivation of the rotor motion equation of multimachine at Section V-A in this article, the damping torque analysis can be applied to the multimachine system. The linearized generator rotor motion equation for the ith generator is given by

$$T_{Ji}\frac{\mathrm{d}\Delta\omega}{dt} = \Delta P_{mi} - \Delta P_{ei} - D_i\Delta\omega. \tag{C1}$$

Based on the fact that $\Delta\omega$ of each generator is the same during ULFO and considering the definition of K_i at Section V-A of this article, the rotor motion equations of all hydropower generators can be added together as follows:

$$\sum_{i=1}^{5} K_i T_{Ji}\frac{\mathrm{d}\Delta\omega}{dt} = \sum_{i=1}^{5}\left(K_i\Delta P_{mi} - K_i\Delta P_{ei} - K_i D_i\Delta\omega\right). \tag{C2}$$

Based on the damping torque theory, $\Delta P_{\mathrm{m}i}$ and ΔP_{ei} can also be decomposed into

$$\begin{cases}\Delta P_{mi} = -D_{mi}\Delta\omega - K_{mi}\Delta\delta \\ \Delta P_{ei} = D_{ei}\Delta\omega + K_{ei}\Delta\delta.\end{cases} \tag{C3}$$

Substituting (C3) into (C2), it can be derived that

$$\begin{aligned}\sum_{i=1}^{5} K_i T_{Ji}\frac{\mathrm{d}\Delta\omega}{dt} = &\sum_{i=1}^{5} K_i\left(D_{mi} + D_{ei} + D_i\right)\Delta\omega \\ &- \sum_{i=1}^{5} K_i\left(K_{mi} + K_{ei}\right)\Delta\delta\end{aligned}$$

$$D_\Sigma = \sum_{i=1}^{5} K_i\left(D_{mi} + D_{ei} + D_i\right). \tag{C4}$$

To calculate the specific value of damping torques, a set of hydropower generator parameters is shown in Table XVI.

Based on the parameters in Table XVI and (C2) and (C4), the damping torque position diagram of the multimachine system in this case can be drawn, as shown in Fig. 19, which is similar

TABLE XV
PARAMETERS OF HYDROPOWER GENERATOR

	Capacity	T_J	T_W	K_P	K_I	b_p	T_d
Weak damping	100 MW	6 s	1.8 s	1.3	0.3	0.01	0.02 s
Strong damping	100 MW	6 s	1.5 s	1.2	0.23	0.01	0.02 s
Negative damping	100 MW	6 s	2 s	1.5	0.4	0.01	0.02 s

TABLE XVI
PARAMETERS OF HYDROPOWER GENERATORS UNDER NEGATIVE DAMPING CONDITION

Generator	T_J	T_W	K_P	K_I	b_p	T_d
YJW	6.5 s	1.8 s	1.2	0.42	0.01	0.02 s
MP	5 s	1.5 s	1.3	0.44	0.01	0.02 s
CCB	6 s	1.5 s	1.2	0.42	0.01	0.02 s
HJQ	8 s	2 s	1	0.4	0.01	0.02 s
MGQ	4.5 s	1.2 s	1.3	0.44	0.01	0.02 s

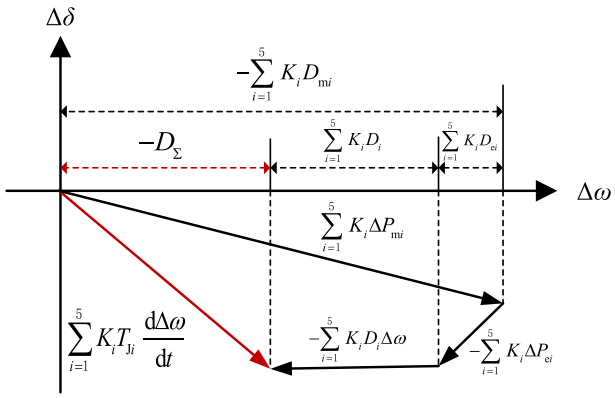

Fig. 19. Decomposition on the $\Delta\omega$–$\Delta\delta$ plane for the terms in the rotor motion equations of the multimachine system with five hydropower generators.

with that of the single machine system. The total damping torque of the system is $D_\Sigma = \sum_{i=1}^{5} K_i(D_{mi} + D_{ei} + D_i)$. A bigger D_Σ indicates a higher system damping. The system stability condition is that $D_\Sigma > 0$. Define $D_{m\Sigma} = \sum_{i=1}^{5} K_i D_{mi}$. When $D_{m\Sigma} < 0$, the governor and turbine of all the hydropower generators provide negative damping. From Fig. 19, the governor and turbine of the hydropower generators provide a large negative damping torque, which will cause the overall damping of the system to be negative and lead to system instability.

The specific value of D_Σ in this case is $D_\Sigma = -0.3668 < 0$. Therefore, the system is unstable according to the damping torque theory. Fig. 20 shows the corresponding time domain simulation result of the system frequency in this case, which is without PV and its supplementary damping control. From Fig. 20, the system is unstable and the frequency diverges. Therefore, the simulation result is consistent with the damping torque analysis result.

To further analyze the damping torque characteristics of this multimachine system, the result of D_{mi} (i = YJW, HJQ, MP, MGQ, and CCB) and $D_{m\Sigma}$ with the variation of frequencies are shown in Fig. 21. From Fig. 21, it can be deduced that 1) the

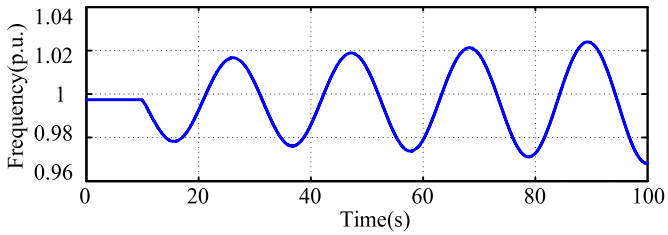

Fig. 20. Time domain simulation result of the system frequency without PV supplementary damping control.

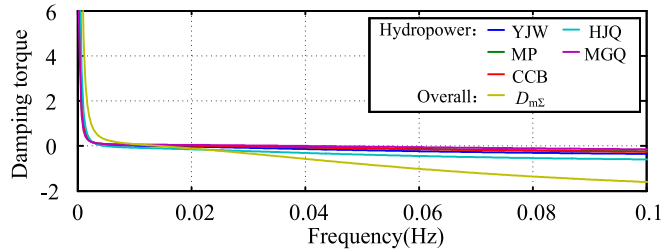

Fig. 21. Damping characteristic of D_{mi} (i = YJW, HJQ, MP, MGQ, and CCB) and $D_{m\Sigma}$ for the multimachine system without PV and its supplementary damping control.

damping torque of each hydropower generator is negative for the ultralow frequency band (0.01–0.1 Hz), 2) $D_{m\Sigma}$ exhibits the largest negative damping torque due to its aggregation of the five hydropower generators, and 3) the hydropower generator HJQ provides the largest negative damping torque due to its largest capacity and biggest water hammer effect time constant.

B. Analysis for the System With Five Hydropower Generators and 2 PV Stations

This section further analyzes the ULFO of the multimachine system with five hydropower generators and two PV stations considering the proposed PV supplementary damping control.

Based on the formulation at Section V-A in this article, (C4) can be rewritten as (C5) after adding two PVs, given by

$$\sum_{i=1}^{5} K_i T_{Ji} \frac{d\Delta\omega}{dt} = \sum_{i=1}^{5} (K_i \Delta P_{mi} - K_i \Delta P_{ei} - K_i D_i \Delta\omega) + \frac{1}{S_\Sigma} \sum_{j=1}^{2} \Delta P'_{PVj} \tag{C5}$$

According to Section IV of this article, the output power of PV can be expressed as

$$\Delta P'_{PVj} = D_{PVj} \Delta\omega. \tag{C6}$$

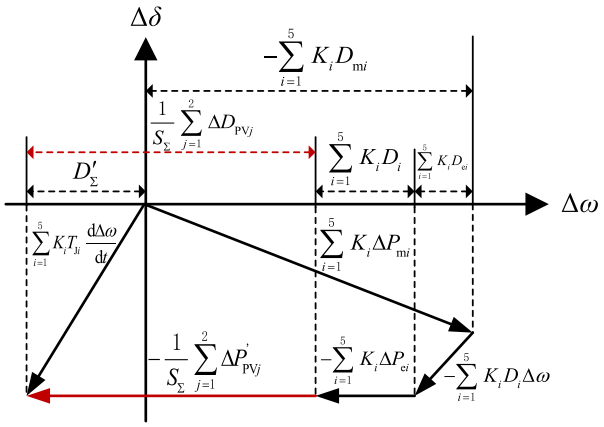

Fig. 22. Decomposition on the $\Delta\omega$–$\Delta\delta$ plane for the terms in the rotor motion equations of the multimachine system with five hydropower generators and two PV stations.

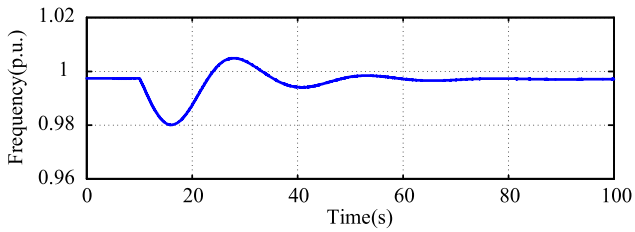

Fig. 23. Time domain simulation of the system frequency with PV supplementary damping control.

Substituting (C6) and (C3) into (C5) yields

$$\sum_{i=1}^{5} K_i T_{Ji}\frac{d\Delta\omega}{dt} = \sum_{i=1}^{5} K_i\left(D_{mi}+D_{ei}+D_i\right)\Delta\omega + \frac{1}{S_\Sigma}\sum_{j=1}^{2} D_{PVj}\Delta\omega - \sum_{i=1}^{5} K_i\left(K_{mi}+K_{ei}\right)\Delta\delta$$

$$D'_\Sigma = \sum_{i=1}^{5} K_i\left(D_{mi}+D_{ei}+D_i\right) + \frac{1}{S_\Sigma}\sum_{j=1}^{2}\Delta D_{PVj}. \quad \text{(C7)}$$

The proposed PV supplementary damping control regulates the PV output power P_{PV} by controlling the dc voltage U_{dc} of the PV array. Furthermore, U_{dc} is controlled to be changed according to the system frequency ω. Therefore, P_{PV} is correspondingly regulated based on the system frequency ω, and the PV system can provide positive damping torque for ULFO. According to (C7), the damping torque diagram for the studied system is shown in Fig. 22. Compared with Fig. 19, the effect of the PV damping torque, i.e., $\frac{1}{S_\Sigma}\sum_{j=1}^{2}\Delta D_{PVj}$, can be observed. The overall damping torque D'_Σ becomes a positive value. Based on the given parameters, D'_Σ is calculated to be $1.1609 > 0$, indicating a stable system. Fig. 23 shows the time domain simulation result of the system frequency in this case. The simulation result also indicates a stable system, which is consistent with the above damping torque analysis result.

To further analyze the damping torque characteristics of this multimachine system, the result of D_{mi} (i = YJW, HJQ, MP, MGQ, and CCB, they are hydropower generators), ΔD_{PVj} (j = XNH and MX, they are PV stations) and $D_{m\Sigma}+D_{PV}$ with the variation of frequencies are shown in Fig. 24. Note that $\frac{1}{S_\Sigma}\sum_{j=1}^{2}\Delta D_{PVj}$ is defined as D_{PV}.

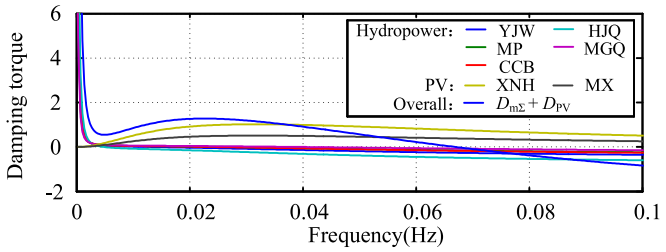

Fig. 24. Damping characteristic line with PV supplementary damping control.

A comparison between Figs. 21 and 24 indicates that 1) the damping torques provided by PV stations XNH and MX are positive for the ULFO frequency band, and 2) the overall damping torque $D_{m\Sigma}+D_{PV}$ thus becomes positive, reflecting the damping effect of PV stations.

C. Analysis for the Influence of Hydropower Generator Parameters on the ULFO

For the multimachine system shown in Fig. 11 of this article, the influence of hydropower generator parameters on the ULFO is further analyzed based on the damping torque theory.

Based on the formulation of $D_{m\Sigma}$ ($D_{m\Sigma}=\sum_{i=1}^{5} K_i D_{mi}$) in the above section, the damping torque characteristic curves of $D_{m\Sigma}$ under different T_w, K_p, and K_i are shown Fig. 25(a)–(c), respectively. Note that T_w is the water hammer time constants, and K_p and K_i are the proportional and integral parameters of the governor of hydropower generators. In Fig. 25, T_w, K_p, and K_i for all the hydropower generators are uniformly magnified by a factor of 1–4 based on the basic parameters shown in Table XVI to study the influence of their variations. From Fig. 25(a), the increase of T_w from T_w to $4T_w$ will cause the increase of oscillation frequency and negative damping torque. From Fig. 25(b), the increase of K_p has different effect on the damping torque under different frequencies. From Fig. 25(c), the increase of K_i will generally result in a larger negative damping torque.

APPENDIX D

In this Appendix, we first illustrate how to use our constructed unified frequency response model to calculate the eigenvalues of the multihydropower and multi-PV systems. Then, we elaborated on how to use the small-signal state-space modeling method, which is a well-known analytical tool/method for the analysis of small-signal stability problem, to calculate the system eigenvalues. Subsequently, we compare the eigenvalues obtained from the above two methods to check if they are consistent. In this way, our proposed frequency response model and PV supplementary control method can be proved analytically.

A. System Eigenvalues Calculating Method based on our Frequency Response Model

Our constructed unified frequency response model for multihydropower and multi-PV systems presented in Section V of this article can be presented as shown in Fig. 26.

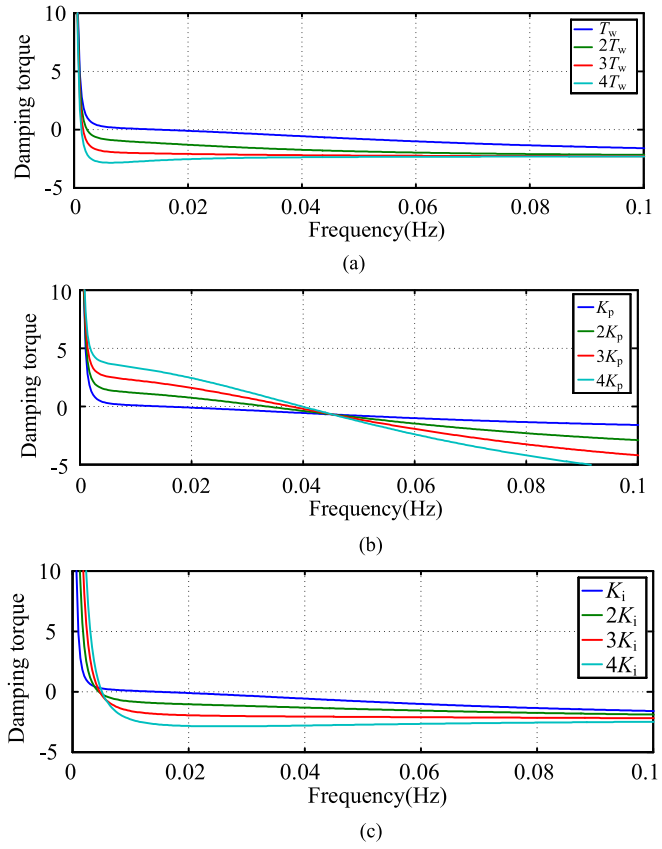

Fig. 25. Damping torque characteristic of $D_{m\Sigma}=\sum_{i=1}^{5}K_iD_{mi}$ under different T_w, K_p, and K_i. (a) Water hammer time constants increase. (b) Gain coefficients increase. (c) Integral coefficients increase.

According to Fig. 26, the transfer function of the whole system can be derived as (D1) shown at the bottom of this page.

Based on (D1), the eigenvalues of the multihydropower and multi-PV system can be obtained by calculating the roots of $1+G(s)=0$. It should be noted that compared with the traditional method, which needs to formulate the small-signal state-space model of the whole system and then calculate the eigenvalues of the state-space matrix A, our above method takes the advantage of the fact that ULFO is the synchronous oscillation of the whole system frequency. Therefore, our modeling complexity of formulating (D1) is greatly reduced.

B. Formulation of the Small-Signal State-Space Model of Multihydropower and Multi-PV System and Corresponding Eigenvalues Calculating Method

The small-signal state-space modeling method is a commonly used analytical tool to analyze the small-signal stability problem of power systems. In this section, the detailed small-signal state-space modeling process of the multihydropower and multi-PV system is provided as follows.

1) Modeling of Hydropower Generators: The hydropower generators are synchronous generators with a fourth-order model. The model is shown as

$$\begin{aligned}\Delta\dot{\delta}&=\omega_0\Delta\omega\\ \Delta\dot{\omega}&=\left(\Delta P_m-\Delta P_e-D\left(1-\Delta\omega\right)\right)/T_{\mathrm{J}}\\ \Delta\dot{E}_q'&=\left(-\Delta E_q'-\left(X_d-X_d'\right)\Delta I_d+\Delta E_{fd}\right)/T_{d0}'\\ \Delta\dot{E}_d'&=\left(-\Delta E_q'+\left(X_q-X_q'\right)\Delta I_q\right)/T_{q0}'\end{aligned}\tag{D2}$$

where ω_0 is the base angular frequency, T_{J} is the inertia constant, P_m is the mechanical power, P_e is the electromagnetic power, D is the damping coefficient, $E^{'}{}_d$ and $E^{'}{}_q$ are the d-axis and q-axis transient voltages, respectively, X_d and X_q are the unsaturated reactances, $X^{'}{}_d$ and $X^{'}{}_q$ are the unsaturated transient reactances, I_d and I_q are the d-axis and q-axis currents, respectively, E_{fd} is the excitation voltage, and $T^{'}{}_{d0}$ and $T^{'}{}_{q0}$ are the unsaturated subtransient times.

To study ULFO, a detailed model of a governor and a turbine is selected. It is consisted of a regulating system, an electro-hydraulic servo system, and a turbine model, given by

$$\begin{cases}\Delta\dot{x}_1=-K_I\Delta\omega-K_Ib_p\Delta x_1\\ \Delta\dot{y}=-\frac{K_P}{T_G}\Delta\omega+\frac{1-K_Pb_p}{T_G}\Delta x_1-\frac{1}{T_G}\Delta y\\ \Delta\dot{P}_m=\frac{2K_P}{T_G}\Delta\omega+\frac{2K_Pb_p-2}{T_G}\Delta x_1+\frac{2T_W+2T_G}{T_GT_W}\Delta y\\ \qquad\quad-\frac{2}{T_W}\Delta P_m\end{cases}\tag{D3}$$

where Δx_1 is the state variable of the integral link of the PID governor, Δy is the change of guide vane opening, and ΔP_m is the change of mechanical power.

A typical fourth-order excitation system modeled as

$$\begin{aligned}\Delta\dot{U}_{ex1}&=(\Delta U_m-\Delta U_{ex1})/T_r\\ \Delta\dot{U}_{ex2}&=\Big(K_a\Big(\Delta U_{\mathrm{ref}}+\Delta U_{\mathrm{PSS}}-\Delta U_{ex1}-\Delta U_{ex2}\\ &\qquad-\frac{K_f}{T_f}\Delta E_{fd}\Big)-\Delta U_{ex2}\Big)/T_a\\ \Delta\dot{U}_{ex3}&=-\left(K_f\Delta E_{fd}/T_f+\Delta U_{ex3}\right)/T_f\\ \Delta\dot{E}_{fd}&=-\left(\Delta E_{fd}\left(1+\Delta S_e\right)-\Delta U_{ex2}\right)/T_e\end{aligned}\tag{D4}$$

where U_{ex1}, U_{ex2}, and U_{ex3} are selected as the state variables, U_m, U_{ref}, and E_{fd} are the terminal voltage, reference input excitation voltage, and generator excitation potential, respectively, and K_a, K_f, T_a, T_f, T_r, and T_e are the amplifier gain, stabilizer gain, amplifier time constant, stabilizer time constant, measurement time constant, and excitation circuit time constant, respectively. The expressions of S_e and U_{ex} are shown as

$$\Delta S_e=A_e(e^{B_e|E_{fd}|}-1)+A_eB_eE_{fd}e^{B_e|E_{fd}|}\mathrm{sgn}(E_{fd})\tag{D5}$$

$$\begin{cases}\frac{\Delta\omega}{\Delta\omega_{\mathrm{ref}}}=\frac{G(s)}{1+G(s)}G\left(s\right)=\left[\sum_{i=1}^{N}K_iG_{\mathrm{gov}i}\left(s\right)G_{Ti}\left(s\right)+\sum_{j=1}^{M}K_jG_{cj}\left(s\right)G_{\mathrm{PV}j}\left(s\right)K_{\mathrm{PU}j}\left(s\right)\right]\\ \qquad\times\frac{\frac{1}{\sum_{i=1}^{N}K_iT_{Ji}s+\sum_{i=1}^{N}K_iD_i}}{1+\frac{1}{\sum_{i=1}^{N}K_iT_{Ji}s+\sum_{i=1}^{N}K_iD_i}\left[\sum_{i=1}^{N}K_iG_{ei}(s)G_{\mathrm{PSS}i}(s)\right]}.\end{cases}\tag{D1}$$

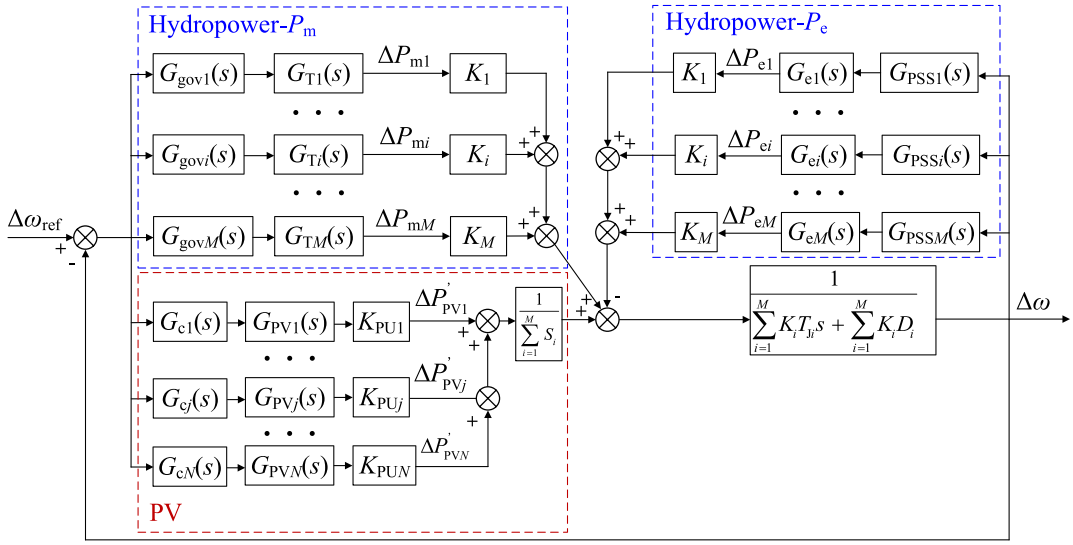

Fig. 26. Unified frequency response model for multihydropower and multi-PV systems.

where A_e is the first-order limiting coefficient, and B_e is the second-order limiting coefficient and sgn is a symbolic function.

The small-signal model of a hydropower generator can be obtained by combining (D2)–(D4), given by

$$\Delta\dot{X}_w = A_{SG}\Delta X_w + B_{SG}\Delta V_{gdq} \tag{D6}$$

where the state variable matrix ΔX_{w} of the hydropower generator is

$$\Delta X_w = \begin{bmatrix} \delta & \omega & E'_q & E'_d & E_{fd} & U_{ex1} & U_{ex2} & U_{ex3}P_m & y & x_1 \end{bmatrix}^T. \tag{D7}$$

The expressions of nonzero coefficients in the coefficient matrix $A_{SG} = [a_{ij}]_{11\times 11}$ are as follows:

$$\begin{aligned}
a_{12} &= \omega_0, a_{22} = -D/2H, a_{29} = 1/2H,\\
a_{33} &= -1/T_{d0}', a_{35} = 1/T_{d0}'\\
a_{44} &= -1/T_{q0}',\\
a_{55} &= -(A_e(e^{B_e|E_{fd}|}-1)\\
&\quad + A_eB_eE_{fd}e^{B_e|E_{fd}|}\mathrm{sgn}(E_{fd})+1)/T_e\\
a_{57} &= 1/T_e, a_{66} = -1/T_r,\\
a_{75} &= -(K_aK_f)/(T_aT_f), a_{76} = -K_a/T_a\\
a_{77} &= -1/T_a, a_{78} = -K_a/T_a,\\
a_{85} &= -K_f/{T_f}^2, a_{88} = -1/T_f\\
a_{92} &= 2K_P/T_G, a_{99} = -2/T_W,\\
a_{9,10} &= (2T_W + 2T_G)/T_GT_W\\
a_{9,11} &= 2K_Pb_p - 2)/T_G,\\
a_{10,2} &= -K_P/T_G, a_{10,10} = -1/T_G\\
a_{10,11} &= (1-K_Pb_p)/T_G,\\
a_{11,2} &= -K_I, a_{11,11} = -b_pK_I.
\end{aligned} \tag{D8}$$

The expressions of nonzero coefficients in the coefficient matrix $B_{\mathrm{SG}} = [b_{ij}]_{11\times 2}$ are as follows:

$$\begin{aligned}
b_{21} &= -(V_{gq}/X_q' + (E_q' - V_{gq})/X_d')/(2H)\\
b_{22} &= (V_{gd}/X_d' + (E_d' - V_{gd})/X_q')/(2H)\\
b_{32} &= -(X_d' - X_d)/(T_{d0}'X_d')\\
b_{41} &= -(X_q' - X_q)/(T_{q0}'X_q').
\end{aligned} \tag{D9}$$

2) Modeling of PV: A PV model mainly includes a PV array, an inverter, and controllers. A practical engineering model of PV is used in this article. The standard conditions for PV cells are $S_{\mathrm{ref}} = 1000\,\mathrm{W/m^2}$ and $T_{\mathrm{ref}} = 25\,^{\circ}\mathrm{C}$. In addition, the voltage–current equation under nonstandard conditions can be descried as

$$\Delta I_{\mathrm{dc}} = -mI_{sc}C_1\frac{1}{nC_2U_{\mathrm{oc}}}e^{\frac{U_{\mathrm{dc}}}{nC_2U_{\mathrm{oc}}}}\Delta U_{\mathrm{dc}}. \tag{D10}$$

The PV controller is consisted of a voltage controller and a current controller, which can achieve main functions. The voltage controller regulated the dc voltage to control or maximize the power extracted from the PV array. The current controller realized the control of an actual current to the current reference value. The small-signal model of the PV controller can be obtained by linearization as following:

$$\begin{aligned}
\Delta\dot{X}_V &= -\Delta U_{\mathrm{dc}}\\
\Delta\dot{Y}_d &= -K_{pv}\Delta U_{\mathrm{dc}} + K_{iv}\Delta X_V - \Delta i_{gd}\\
\Delta\dot{Y}_q &= -\Delta i_{gq}\\
\Delta v_{kd}^* &= K_{pi}\Delta\dot{Y}_d + K_{ii}\Delta Y_d - \omega_nL_f\Delta i_{gq} + \Delta v_{gd}\\
\Delta v_{kq}^* &= K_{pi}\Delta\dot{Y}_q + K_{ii}\Delta Y_q + \omega_nL_f\Delta i_{gd} + \Delta v_{gq}
\end{aligned} \tag{D11}$$

where Δx_{V} is the state variable of the dc voltage controller, and ΔY_d and ΔY_q are the state variables of the current controller.

The equation of the state for the dc capacitor of PV is

$$\Delta\dot{U}_{\rm dc} = \frac{1}{C_{\rm dc}}\Delta I_{\rm dc} - \frac{3}{2}\frac{i_{gd}}{U_{\rm dc}}\Delta v_{gd} - \frac{3}{2}\frac{v_{gd}}{U_{\rm dc}}\Delta i_{gd} + \frac{3}{2}\frac{v_{gd}i_{gd}}{U_{\rm dc}^2}\Delta U_{\rm dc}. \tag{D12}$$

The small-signal model of a PV generator can be obtained by combining (D10)–(D12) as follows:

$$\Delta\dot{X}_{\rm PV} = A_{\rm PV}\Delta X_{\rm PV} + B_{\rm PV}\Delta V_{gdq} \tag{D13}$$

where the state variable matrix $\Delta X_{\rm PV} = [\Delta U_{\rm dc}, \Delta X_V, \Delta Y_d, \Delta Y_q, \Delta i_{gd}, \Delta i_{gq}]^{\rm T}$, and the mathematical expression of the coefficient matrix $A_{\rm PV}$ and $B_{\rm PV}$ are as follows: (D14), shown at the bottom of this page.

$$B_{\rm PV} = \begin{bmatrix} -\frac{3i_{gd}}{2C_{\rm dc}U_{\rm dc}} & 0 & 0 & 0 & 0 & 0 \\ 0 & 0 & 0 & 0 & 0 & 0 \end{bmatrix}^{\rm T}. \tag{D15}$$

3) Modeling of Networks and Loads: Suppose the system has N hydropower generator nodes, M nodes of PV generation, and L other nodes (network nodes and load nodes). The modeling of networks and loads can be expressed by algebraic equations:

$$\begin{bmatrix} \Delta I_{gdq1} \\ \cdots \\ \Delta I_{gdq(N+M)} \\ 0 \\ \cdots \\ 0 \end{bmatrix} = \begin{bmatrix} Y_{11} & Y_{12} \\ Y_{21} & Y_{22} \end{bmatrix} \begin{bmatrix} \Delta V_{gdq1} \\ \cdots \\ \Delta V_{gdq(N+M)} \\ \Delta V_{gdq(N+M+1)} \\ \cdots \\ \Delta V_{gdq(N+M+L)} \end{bmatrix} \tag{D16}$$

where $\Delta I_{{\rm g}dqi}$ is the output current of each hydropower generator and PV, $\Delta V_{{\rm g}dqi}$ is the voltage of each node, Y_{11} and Y_{22} are the self admittances of the generator nodes and the network nodes, and Y_{12} and Y_{21} are the mutual admittances of the generator nodes and network nodes.

By eliminating the L other nodes, the network matrix can be simplified as

$$\begin{bmatrix} \Delta I_{gdq1} \\ \cdots \\ \Delta I_{gdq(N+M)} \end{bmatrix} = (Y_{11} - Y_{12}Y_{22}^{-1}Y_{21}) \begin{bmatrix} \Delta V_{gdq1} \\ \cdots \\ \Delta V_{gdq(N+M)} \end{bmatrix}. \tag{D17}$$

4) Modeling of the Whole Multihydropower and Multi-PV System: Based on the above models, the small-signal model of the whole system with N hydropower generators and M PV generators can be obtained by combining (D6), (D13), and (D17), given by

$$\Delta\dot{X}_{\rm sys} = A_{\rm sys}\Delta X_{\rm sys} \tag{D18}$$

where $\Delta X_{\rm sys} = [\Delta X_{w1}, \ldots, \Delta X_{wN}, \Delta X_{\rm PV1}, \ldots, \Delta X_{{\rm PV}M}]^{\rm T}$, $A_{\rm sys}$ is the complete system state matrix, and $\Delta X_{w1}, \ldots, \Delta X_{wN}$ are the state variables of N hydropower generators, and $\Delta X_{\rm PV1}, \ldots, \Delta X_{{\rm PV}N}$ are the state variables of the M PV generations.

Finally, the system eigenvalues can be obtained by calculating the eigenvalues of $A_{\rm sys}$.

C. Prove Our Proposed Model and Method Analytically by Comparing the System Eigenvalues Obtained from Our Proposed Model and the System Small-Signal State-Space model

In this section, the system with five hydropower generators and two PV stations shown in Fig. 11 of this article is used as the test system for the comparison of eigenvalue results. Based on the parameters in Tables XI–XIII, the system eigenvalues are calculated from our proposed frequency response model and the detailed small-signal state-space model for the conditions of 1) weak damping, strong damping, and negative damping with PV dynamics but without PV supplementary damping control, and 2) weak damping with PV dynamics as well as our proposed PV supplementary damping control. The results of the ULFO mode for the above four conditions are given in Table XVII.

From Table XVII, the eigenvalues from our frequency response model have little difference from those calculated by the detailed small-signal state-space model. In addition, Table XVII also indicates that our PV supplementary damping control can effectively change the system damping from weak damping to strong damping.

Therefore, our proposed frequency response model and PV supplementary damping control method have been proved analytically by the commonly used tool of small-signal state-space modeling method.

D. More Small-Signal Stability Analysis Results

Furthermore, based on the above system eigenvalue calculating method, the influence of parameter variations of hydropower generators on the system small-signal stability can be analyzed.

Fig. 27 shows the root locus of the ULFO mode when the parameters of the hydropower generators change. From Fig. 27, when (a) the water hammer time constants, (b) the proportional coefficients of the governor, and (c) the integral coefficients of the governor increase, the ULFO mode will move to the right half plane. It indicates that increasing these parameters will reduce the damping of the ULFO mode.

APPENDIX E

In this appendix, we provide some simulation results to verify the accuracy validation of the constructed frequency response

$$A_{\rm PV} = \begin{bmatrix} \frac{3v_{gd}i_{gd}}{2C_{\rm dc}U_{\rm dc}^2} - \frac{mI_{sc}[1-C_1(e^{\frac{U_{\rm dc}}{nC_2U_{\rm oc}}}-1)]}{C_{\rm dc}U_{\rm dc}} & 0 & 0 & 0 & -\frac{3v_{gd}}{2C_{\rm dc}U_{\rm dc}} & 0 \\ 1 & 0 & 0 & 0 & 0 & 0 \\ K_{pv} & K_{iv} & 0 & 0 & -1 & 0 \\ 0 & 0 & 0 & 0 & 0 & -1 \\ \frac{K_{pi}K_{pv}}{L_f} & \frac{K_{iv}K_{pi}}{L_f} & \frac{K_{ii}}{L_f} & 0 & -\frac{K_{pi}}{L_f} & 0 \\ 0 & 0 & 0 & \frac{K_{ii}}{L_f} & 0 & -\frac{K_{pi}}{L_f} \end{bmatrix} \tag{D14}$$

TABLE XVII
CALCULATION RESULTS OF EIGENVALUES CORRESPONDING TO ULTRA-LOW FREQUENCY MODE

Condition	Model	Eigenvalues	Oscillation Frequency	Damping ratio
Weak damping	Proposed frequency response model	–0.0318 ± 0.2627i	0.0418 Hz	12.03%
	Small-signal model	–0.0305 ± 0.2676i	0.0426 Hz	11.32%
Strong damping	Proposed frequency response model	–0.0668 ± 0.2378i	0.0378 Hz	27.06%
	Small-signal model	–0.0651 ± 0.2402i	0.0382 Hz	26.16%
Negative damping	Proposed frequency response model	0.0039 ± 0.2991i	0.0476 Hz	–1.3%
	Small-signal model	0.0032 ± 0.3011i	0.0479 Hz	–1.06%
Weak damping with PV supplementary damping control	Proposed frequency response model	–0.0816 ± 0.2594i	0.0413 Hz	30%
	Small-signal model	–0.0801 ± 0.2618i	0.0417 Hz	29.26%

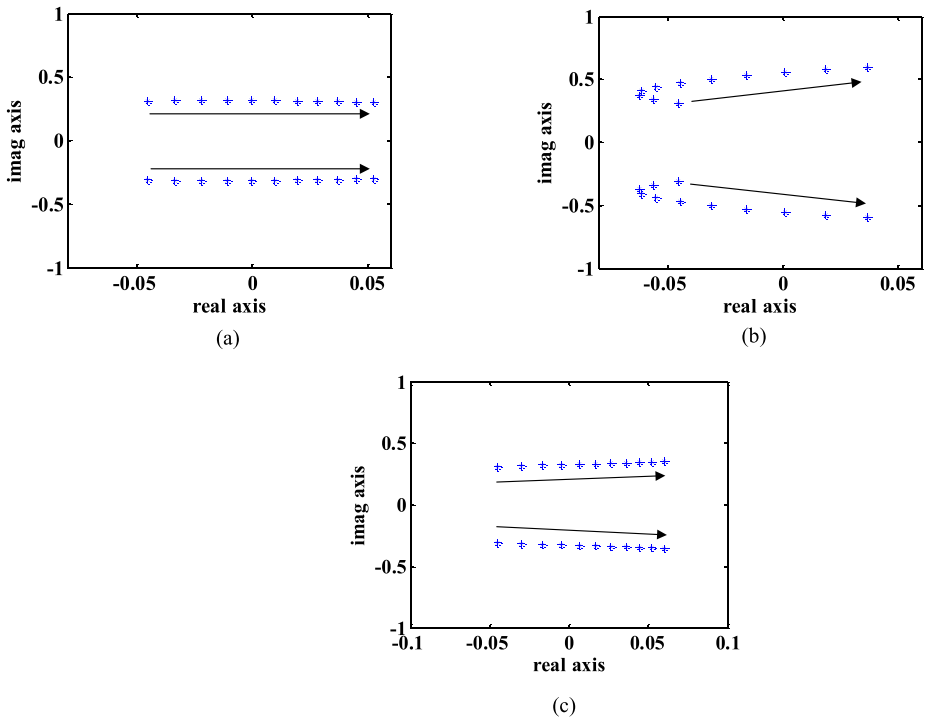

Fig. 27. Root locus of the ULFO mode when the parameters of the hydropower generators change. (a) Water hammer time constants increase. (b) Proportional coefficient of the governor increase. (c) Integral coefficient of the governor increase.

TABLE XVIII
CALCULATION RESULTS OF EIGENVALUES CORRESPONDING TO ULTRA-LOW FREQUENCY MODE

Condition	Eigenvalues	Oscillation Frequency	Damping ratio
Weak damping	–0.032 ± 0.263i	0.0418 Hz	12.03%
Strong damping	–0.067 ± 0.238i	0.0378 Hz	27.06%
Negative damping	0.004 ± 0.299i	0.0476 Hz	–1.3%
Weak damping with PV damping control	–0.082 ± 0.259i	0.0413 Hz	30%

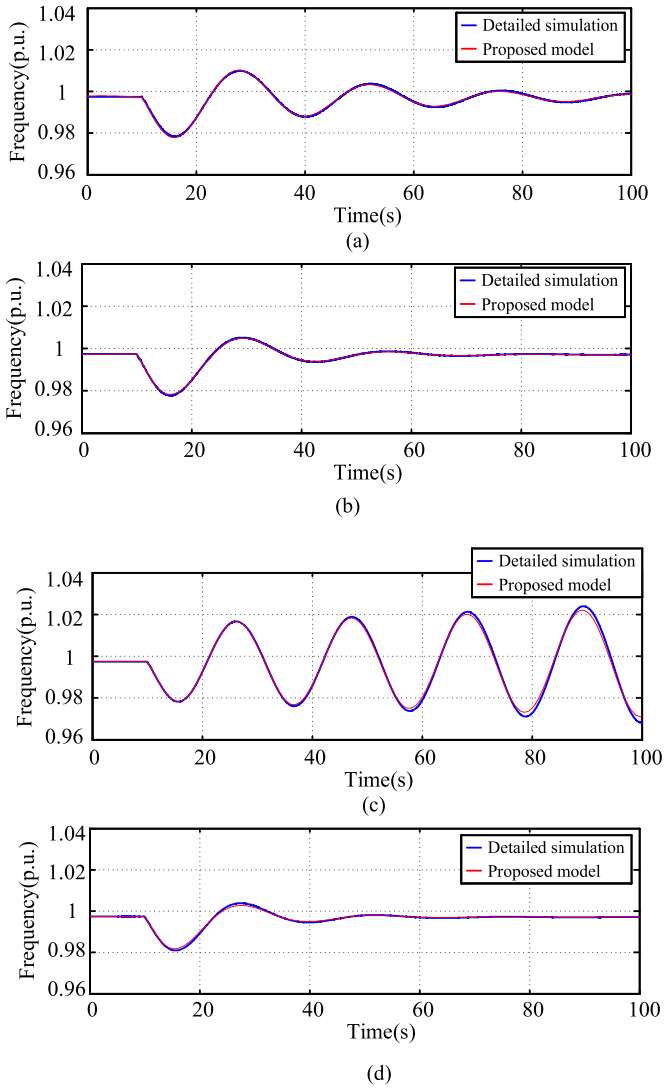

Fig. 28. Comparison results of the multimachine system: the response of the system frequency obtained from our proposed frequency response model and the detailed time-domain simulation. (a) Weak damping. (b) Strong damping. (c) Negative damping. (d) Weak damping with PV supplementary damping control.

model. Three parameter conditions of weak damping, strong damping, and negative damping of the studied multimachine system are set, respectively, for analysis, and Tables XII–XIV in Appendix B show these different parameters.

Based on the parameters in Tables XII–XIV, the response of the system frequency is obtained from our proposed frequency response model and the detailed time-domain simulation for the conditions of 1) weak damping, strong damping, and negative damping with PV dynamics but without PV supplementary damping control, and 2) weak damping with PV dynamics as well as our proposed PV supplementary damping control. Fig. 28(a)–(d) shows the comparison results for the above four conditions, respectively. The small-signal disturbance is a load increase of 10 MW. From Fig. 28, the two responses are consistent with each other, thus validating the accuracy of our frequency response model. In addition, Fig. 28(d) also indicates that

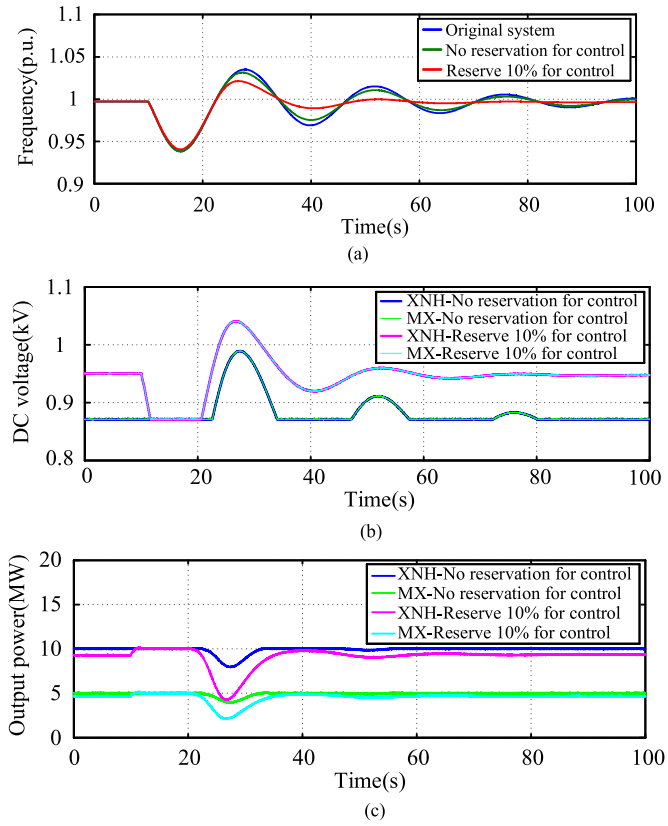

Fig. 29. Simulation results for the cases of reserving 10% of PV maximum output power capability and not reserving power (always works at MPPT point). (a) System frequency. (b) PV DC voltage. (c) PV output power.

our PV supplementary damping control can effectively change the system damping from weak damping to strong damping.

For the above four conditions, the system eigenvalues are calculated from our frequency response model. The results of ULFO mode are shown in Table XVIII. From Table XVIII and Fig. 28, the calculated ULFO modes of each condition are consistent with the time-domain simulation results, which proves the accuracy of our eigenvalue calculating method.

Appendix F

In this appendix, we provide a simulation comparison of the suppression effect of PV on the ULFO with or without reserving PV power. The supplementary control gain K_c is set to the same value in both cases. The test system is shown in Fig. 11 with five hydropower generators and two PV stations, and the disturbance is a load change of 30 MW.

Fig. 29(a) shows the system frequency results. The blue line is the case without PV supplementary control. The green line is the case when PV always works at the maximum power point (no reservation). The red line is the case when 10% of the PV maximum output power capability is reserved. From Fig. 29(a), the PV supplementary damping control can also suppress the ULFO without reservation. If 10% is reserved for control, the suppression effect is better. Fig. 29(b) and (c) shows the responses of PV dc voltage and output power, respectively. XNH and MX denote the names of the two PV stations.

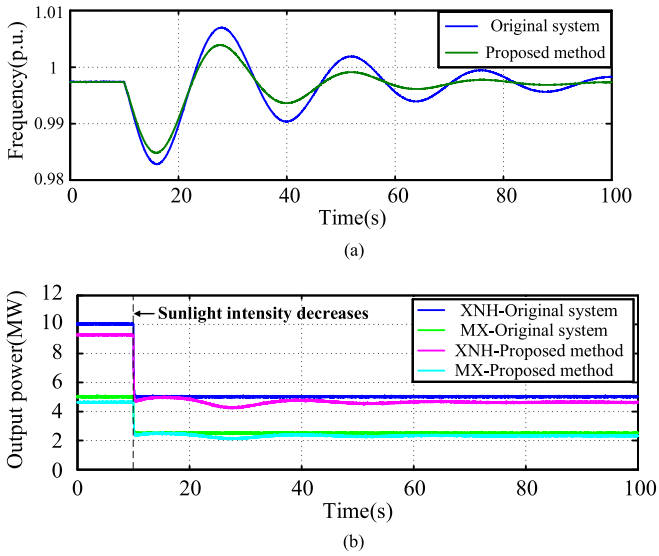

Fig. 30. Simulation results for the change of the sunlight intensity. (a) System frequency. (b) PV output power.

Fig. 29(b) indicates that the PVs' dc voltages will change during the suppression process. Fig. 29(c) indicate that when there is no reservation, PVs can only suppress ULFO by reducing the output power. When 10% is reserved for control, PVs can also increase the output power to suppress ULFO, which can provide stronger damping to the system.

In sum, even if the PV works at the maximum power point, it can still suppress the ULFO.

APPENDIX G

In this appendix, we provide a simulation result to test the influence of intermittency characteristics of PV output power. The multimachine system with five hydropower generators and two PV stations shown in Fig. 11 of this article is used for simulation tests. Initially, the total load in the system is 105 MW. At $t = 10$ s, the sunlight intensity changes from 1000 to 500 W/m^2, and the PV's power also decreases. Fig. 30 compares the simulation results without damping control and with the proposed PV supplementary damping control method. The responses of system frequency and output active power of XNH and MX PV are, respectively, shown in Fig. 30(a) and (b). As can be seen from Fig. 30, due to the reduction of PV's output power, the system occurs ULFOs after $t = 10$ s. But our proposed method can regulate the PV' output power in the following dynamic process according to the system frequency and thus participate in mitigating the ULFO.

The above results validate that our proposed PV supplementary controller can still have a desirable damping effect considering the intermittent characteristic of PV output power.

REFERENCES

[1] S. V. Papaefthymiou, E. G. Karamanou, S. A. Papathanassiou, and M. P. Papadopoulos, "A wind-hydro-pumped storage station leading to high RES penetration in the autonomous island system of Ikaria," *IEEE Trans. Sustain. Energy*, vol. 1, no. 3, pp. 163–172, Oct. 2010.

[2] Y. Qiu, J. Lin, F. Liu, Y. Song, G. Chen, and L. Ding, "Stochastic online generation control of cascaded Run-of-the-river hydropower for mitigating solar power volatility," *IEEE Trans. Power Syst.*, vol. 35, no. 6, pp. 4709–4722, Nov. 2020.

[3] H. N. Villegas Pico, D. C. Aliprantis, J. D. McCalley, N. Elia, and N. J. Castrillon, "Analysis of hydro-coupled power plants and design of robust control to damp oscillatory modes," *IEEE Trans. Power Syst.*, vol. 30, no. 2, pp. 632–643, Mar. 2015.

[4] H. Villegas Pico, J. D. McCalley, A. Angel, R. Leon, and N. J. Castrillon, "Analysis of very low frequency oscillations in hydro-dominant power systems using multi-unit modeling," *IEEE Trans. Power Syst.*, vol. 27, no. 4, pp. 1906–1915, Nov. 2012.

[5] L. Sun and X. Zhao, "Modelling and analysis of frequency-responsive wind turbine involved in power system Ultra-low frequency oscillation," *IEEE Trans. Sustain. Energy*, vol. 13, no. 2, pp. 844–855, Apr. 2022.

[6] X. Shi et al., "Analysis of ultra-low frequency oscillation in hydro-dominant power system and suppression strategy by GPSS," *IEEE Trans. Ind. Appl.*, vol. 59, no. 3, pp. 2796–2806, May/Jun. 2023.

[7] G. Chen et al., "Optimization strategy of hydrogovernors for eliminating ultralow-frequency oscillations in hydrodominant power systems," *IEEE J. Emerg. Sel. Topics Power Electron.*, vol. 6, no. 3, pp. 1086–1094, Sep. 2018.

[8] L. Chen et al., "Optimization of governor parameters to prevent frequency oscillations in power systems," *IEEE Trans. Power Syst.*, vol. 33, no. 4, pp. 4466–4474, Jul. 2018.

[9] G. Zhang et al., "Deep reinforcement learning-based approach for proportional resonance power system stabilizer to prevent ultra-low-frequency oscillations," *IEEE Trans. Smart Grid*, vol. 11, no. 6, pp. 5260–5272, Nov. 2020.

[10] H. Ghasemi and C. Canizares, "On-line damping torque estimation and oscillatory stability margin prediction," *IEEE Trans. Power Syst.*, vol. 22, no. 2, pp. 667–674, May 2007.

[11] S. C. Chevalier, P. Vorobev, and K. Turitsyn, "Using effective generator impedance for forced oscillation source location," *IEEE Trans. Power Syst.*, vol. 33, no. 6, pp. 6264–6277, Nov. 2018.

[12] L. Chen et al., "Online emergency control to suppress frequency oscillations based on damping evaluation using dissipation energy flow," *Int. J. Electric Power Energy Syst.*, vol. 103, pp. 414–420, 2018.

[13] T. Chaiyatham and I. Ngamroo, "Improvement of power system transient stability by PV farm with fuzzy gain scheduling of PID controller," *IEEE Syst. J.*, vol. 11, no. 3, pp. 1684–1691, Sep. 2017.

[14] R. K. Varma and M. Akbari, "Simultaneous fast frequency control and power oscillation damping by utilizing PV solar system as PV-STATCOM," *IEEE Trans. Sustain. Energy*, vol. 11, no. 1, pp. 415–425, Jan. 2020.

[15] M. Basu, V. R. Mahindara, J. Kim, R. M. Nelms, and E. Muljadi, "Comparison of active and reactive power oscillation damping with PV plants," *IEEE Trans. Ind. Appl.*, vol. 57, no. 3, pp. 2178–2186, May/Jun. 2021.

[16] Y. Zhu, C. Liu, K. Sun, D. Shi, and Z. Wang, "Optimization of battery energy storage to improve power system oscillation damping," *IEEE Trans. Sustain. Energy*, vol. 10, no. 3, pp. 1015–1024, Jul. 2019.

[17] G. Lin et al., "A virtual inertia and damping control to suppress voltage oscillation in islanded DC microgrid," *IEEE Trans. Energy Convers.*, vol. 36, no. 3, pp. 1711–1721, Sep. 2021.

[18] L. Shi, K. Y. Lee, and F. Wu, "Robust ESS-based stabilizer design for damping inter-area oscillations in multimachine power systems," *IEEE Trans. Power Syst.*, vol. 31, no. 2, pp. 1395–1406, Mar. 2016.

[19] G. Tu, Y. Li, and J. Xiang, "Sliding mode control of energy storage systems for reshaping the accelerating power of synchronous generators," *IEEE Trans. Power Syst.*, vol. 38, no. 2, pp. 1242–1256, Mar. 2023.

[20] Q. Yang, L. Yan, X. Chen, Y. Chen, and J. Wen, "A distributed dynamic inertia-droop control strategy based on multi-agent deep reinforcement learning for multiple paralleled VSGs," *IEEE Trans. Power Syst.*, vol. 38, no. 6, pp. 5598–5612, Nov. 2023.

[21] P. Kundur, *Power System Stability and Control*. New York, NY, USA: McGraw-Hill, 1994.

[22] G. Zhang et al., "A multiagent deep reinforcement learning-enabled dual-branch damping controller for multimode oscillation," *IEEE Trans. Control Syst. Technol.*, vol. 31, no. 1, pp. 483–492, Jan. 2023.

[23] M. G. Villalva, J. R. Gazoli, and E. R. Filho, "Comprehensive approach to modeling and simulation of photovoltaic arrays," *IEEE Trans. Power Electron.*, vol. 24, no. 5, pp. 1198–1208, May 2009.

[24] X. Bao, F. Zhuo, Y. Tian, and P. Tan, "Simplified feedback linearization control of three-phase photovoltaic inverter with an LCL filter," *IEEE Trans. Power Electron.*, vol. 28, no. 6, pp. 2739–2752, Jun. 2013.

[25] W. Mo et al., "Analysis and measures of ultra-low frequency oscillations in a large-scale hydropower transmission system," *IEEE J. Emerg. Sel. Topics Power Electron.*, vol. 6, no. 3, pp. 1077–1085, Sep. 2018.

Sijia Wang received the B.E. degree in building electricity and intelligence from the Qingdao University of Technology, Qingdao, China, in 2016, and the M.S. degree in electrical engineering in 2020 from Beijing Jiaotong University, Beijing, China, where he is currently working toward the Ph.D. degree in electrical engineering.

His research interests include power system stability analysis and control.

Yin Xu (Senior Member, IEEE) received the B.E. and Ph.D. degrees in electrical engineering from Tsinghua University, Beijing, China, in 2008 and 2013, respectively.

From 2013 to 2016, he was an Assistant Research Professor with the School of Electrical Engineering and Computer Science, Washington State University, Pullman, WA, USA. He is currently a Professor with the School of Electrical Engineering, Beijing Jiaotong University, Beijing. His research interests include power grid resilience, power system electromagnetic transient modeling, and high-performance simulation.

Dr. Xu is currently the Chair of the Energy Internet Resilience Working Group under the IEEE PES Energy Internet Coordinating Committee and Secretary of the Distribution Test Feeder Working Group under the IEEE PES Distribution System Analysis Subcommittee. He is an Editorial Broad Member of IEEE TRANSACTIONS ON POWER SYSTEMS, IEEE POWER ENGINEERING LETTERS, *IET Smart Grid*, and *Energy Conversion and Economics*.

Xiangyu Wu (Senior Member, IEEE) received the B.S. degree from the Department of Electrical Engineering, Zhejiang University, Hangzhou, China, in 2012, and the Ph.D. degree in electrical engineering from Tsinghua University, Beijing, China, in 2017.

He is currently an Associate Professor with the School of Electrical Engineering, Beijing Jiaotong University, Beijing. In 2015, he was a Visiting Scholar with the University of Toronto, Toronto, ON, Canada. In 2019, he was a Guest Researcher with the Department of Energy Technology, Aalborg University, Aalborg, Denmark. His research interests include operation and control of microgrids, wide-band oscillations of renewable energy-based power systems, and power grid resilience.

Jiaxuan Wang received the B.E. degree from the China University of Geosciences, Beijing, China, in 2020, and the M.S. degree from Beijing Jiaotong University, Beijing, in 2023, both in electrical engineering.

She is currently an Engineer with the State Grid Henan Electric Power Research Institute, Chengdu, China. Her research focuses on power system stability analysis and control.

Gang Chen received the B.S. degree in electrical engineering from Tianjin University, Tianjin, China, in 2008, and the Ph.D. degree in electrical engineering from Tsinghua University, Beijing, China, in 2013.

From 2010 to 2011, he was a Guest Ph.D. Student with the School of Electrical Engineering and Computer Science, Washington State University, Pullman, WA, USA. He is currently a Senior Engineer with the State Grid Sichuan Electric Power Research Institute, Chengdu, China. His research interests include power system dynamic monitoring and control based on wide-area signals, power system frequency stability analysis and control, low and ultra-low frequency oscillation analysis and control, etc.

Xueyang Zeng received the B.S. and Ph.D. degrees in electrical engineering from the College of Electrical Engineering, Sichuan University, Chengdu, China, in 2016 and 2020, respectively.

From 2018 to 2019, he was a Visiting Ph.D. Student with the Department of Energy Technology, Aalborg University, Aalborg, Denmark. He is currently an Engineer with the State Grid Sichuan Electric Power Research Institute, Chengdu. His research interests include renewable energy integration and high-voltage direct current transmission technologies.